2017

Utilizing Single-Molecule Fret Methods to Study Conformational Changes in Trim5α

Margret Suzanne Bradley
Loyola University Chicago

LOYOLA UNIVERSITY CHICAGO

UTILIZING SINGLE-MOLECULE FRET METHODS TO STUDY CONFORMATIONAL CHANGES IN TRIM5α

A THESIS SUBMITTED TO

THE FACULTY OF THE GRADUATE SCHOOL IN CANDIDACY FOR THE DEGREE OF

MASTER OF SCIENCE

PROGRAM IN MICROBIOLOGY AND IMMUNOLOGY

BY

MARGRET SUZANNE BRADLEY

CHICAGO, ILLINOIS

DECEMBER 2017

TABLE OF CONTENTS

LIST OF FIGURES

ABSTRACT

Single-molecule FRET (smFRET) is a method by which dynamic conformational changes in a protein can be monitored microscopically and in real time. smFRET relies on the creation of FRET (Förster Resonance Energy Transfer) between small molecule fluorophores conjugated to the biomolecules of interest. FRET efficiency allows calculation of interfluorophore distances. Changes in FRET efficiency represent changes in protein conformation caused by parts of the protein shifting further apart or closer together which can inform further structural and molecular studies of the protein of interest. For example, in the Campbell Lab, we study the protein TRIM5α, an antiretroviral cellular protein which can cause premature dissociation of the HIV capsid core by an unknown mechanism. We can conjugate small fluorophores to specific sites chosen on TRIM5α or isolated TRIM5α domains and use smFRET to observe conformational changes in TRIM5α that may correlate to disruption of the viral core. Fluorophore conjugation can be done several ways, but we will focus on the use of cysteines to conjugate maleimide-linked fluorophores to our protein of interest.

For my thesis, I propose to adapt and optimize a protocol for smFRET usable by the Campbell Lab. To do this, I will first purify, label, and characterize peptides derived from TRIM5α that retain their secondary structure. I will then optimize methods for smFRET

including instrument calibration, setting up the ability to track multiple fluorophores simultaneously, and analysis of smFRET data both to correctly align data and to render final data analyses.

CHAPTER I: INTRODUCTION

Single-Molecule FRET

Single-molecule FRET (smFRET) is a relatively new technique first developed in 1996 that is becoming more accessible to researchers through developments in technology[1]. smFRET allows the researcher to observe dynamic changes in single molecules over time. The technique can be applied to several types of molecules including nucleic acids and proteins. Much work on nucleic acids and proteins already completed has contributed to the understanding of molecular mechanisms such as the function of DNA polymerase and the unfolding of viral envelope proteins[2,3].

smFRET, as the name implies, relies on the principles of FRET (Förster Resonance Energy Transfer). FRET occurs when two fluorophores are close together and one fluorophore, the donor fluorophore, gets excited. Excited fluorophores emit light at a lower energy wavelength than that at which they are excited due to vibrational relaxation. If the two fluorophores are close enough together and designed so that the emission wavelength of the donor fluorophore overlaps with the excitation wavelength of the second fluorophore, the acceptor, then an energy transfer event takes place and the observed light will now be the emission from the acceptor fluorophore (Figure 1)[4]. In the case of the green/red pairing of the fluorophores Alexa

488 and Alexa 594, the green 488 fluorophore can excite the red 594 fluorophore, resulting in red light emission. This energy transfer phenomena is called FRET[4].

For smFRET, small fluorophores are conjugated to the molecules of interest in a site-specific manner and the molecules are observed using microscopy[5].

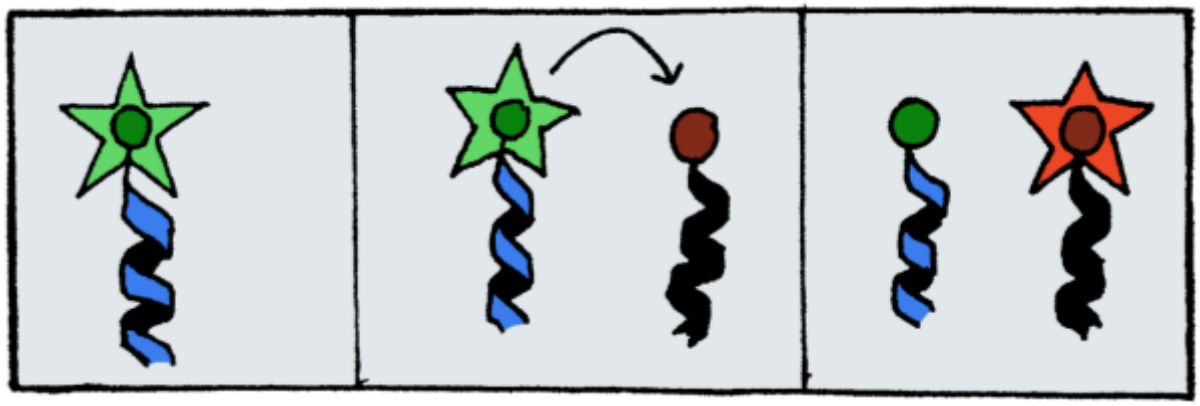

Figure 1. FRET. Diagram of an energy transfer event in FRET. When the red fluorophore come in close proximity of the excited green fluorophore, energy transfers from the green fluorophore to the red fluorophore resulting in dimmer green light observed and a simultaneous increase in red light. Figure hand drawn by Margret Bradley.

Molecule Adherence to Slides.

To do smFRET and get reasonable data, the molecules need to be stationary on the slide[1]. Molecules which are not adhered to the slide may drift in and out of the plane of focus via diffusion, which can complicate data analysis and make resolving conformational changes difficult. Thus, a complicated and important process of slide adherence has been developed. After extensive cleaning to remove residues from old experiments or other contaminants, slides - either quartz or glass - are activated using a silane treatment[6]. The silane treatment allows

reagents such as polyethylene glycol (PEG) to stick to the slide surface[7]. Biotin conjugated to a portion of the PEG molecules provides a surface to which many molecules may be adhered using biotin/streptavidin binding. In our study, we created a layer of neutravidin over the Biotin-PEG and added another layer of biotinylated antibodies which could bind our protein, immobilizing it at the slide surface (Figure 2).

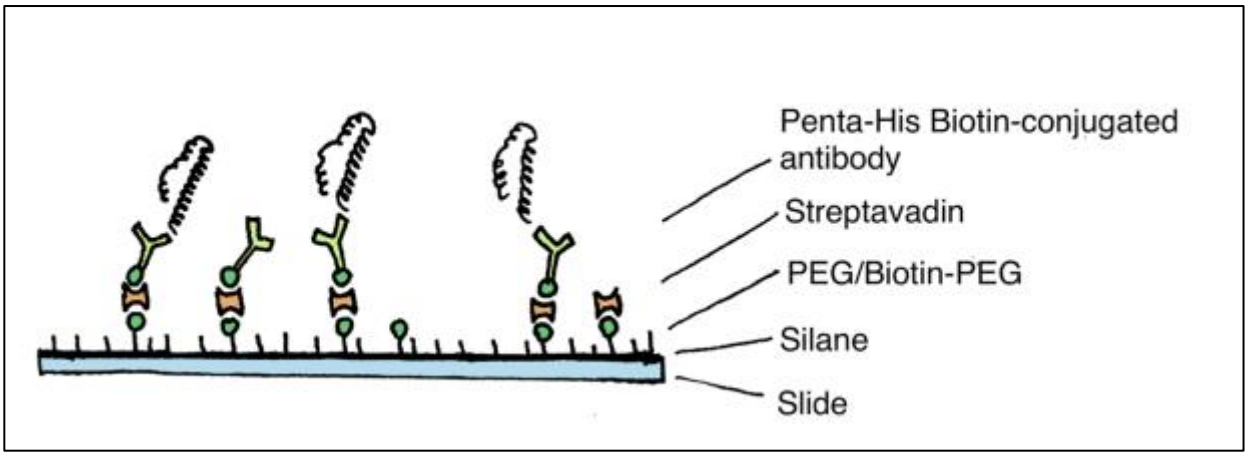

Figure 2. Slide Adhesion. Diagram of the slide coatings used to allow for adhesion of the protein of interest to the slide. The slide surface is activated with 3-aminopropyltriethoxysilane and coated with a mixture of PEG and biotin-conjugated PEG. A layer of streptavadin is applied to the biotinylated PEG and, finally, biotinylated penta-His antibodies are added to bind to the streptavadin. Our His-tagged protein can then be layered on top to complete protein adherence to the slide. Figure hand drawn by Margret Bradley.

TIRF Microscopy.

As smFRET is highly sensitive and detects events occurring on the scale of single molecules, every attempt to limit background noise must be made. Using TIRF (Total Internal Reflection Fluorescence) microscopy limits excitation to only molecules within 100-200nm of the slide surface, such as those tethered there during adhesion of molecules to the slide.[1] In a

solution where particles are not tethered to the surface, fluorescent particles can be seen diffusing in and out of the narrow plane of excitation.

TIRF microscopy is achieved by shining a laser at the sample at a critical angle, wherein the refractive angle of light causes the laser light to be reflected at the sample surface instead of passing through the sample. This allows only a very narrow layer of the sample to be excited by evanescent waves from the laser light and almost completely cuts out background noise from the rest of the sample being studied[8,9]. These properties make TIRF microscopy ideal for smFRET. TIRF microscopy can be set up in two orientations via shining the laser through a prism above the sample (prism TIRF)[10], or shining the laser through the objective lens below the sample (objective TIRF)[8]. Objective TIRF, the method used in our lab, is shown in Figure 3.

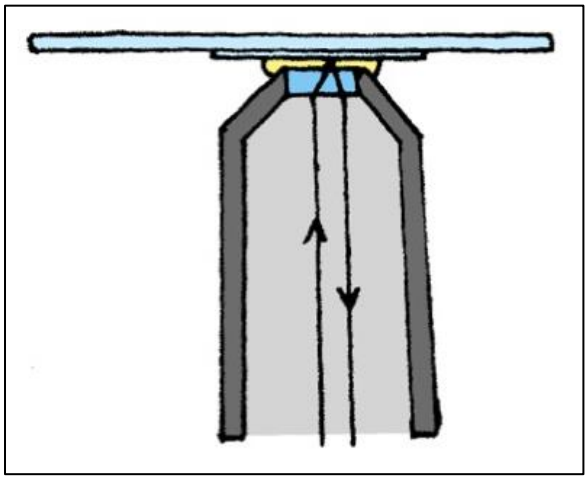

Figure 3. Total Internal Reflection Fluorescence (TIRF). The light path in objective TIRF microscopy. Note the orientation of the microchamber with the coverslip facing downwards. Figure hand drawn by Margret Bradley

smFRET Data Analysis.

Raw smFRET data must go through several layers of analysis before it can be interpreted. The percentage of energy from the donor fluorophore transferred to the acceptor fluorophore is represented as the FRET efficiency. FRET efficiency is calculated using the following equation:

$$E = \left[1 + \gamma \frac{I_D}{I_A}\right]^{-1}$$

where E is the FRET efficiency, I_D is the donor intensity, I_A is the acceptor intensity, and γ is a correction factor to account for differences in detection of donor and acceptor intensity. In true FRET, the FRET efficiency should be between 0 and 1[1]. Fluorophore pairs typically have an R_0 value associated with them where R_0 is the distance between the fluorophores when half the energy of the donor is transferred to the acceptor or E=0.5[11]. R_0 is calculated from the properties of the fluorophores including spectral overlap, quantum yield, and orientational factor. For example, for the fluorophores Alexa 488 and Alexa 594, R_0 is 60Å. We call data tracking light emission intensity over time a trace.

Once the FRET efficiency over time has been calculated for a donor and acceptor FRET pair, further analysis must be done to determine the states present in the trace. Molecules in FRET display multiple levels of FRET efficiency, called states, which translate to different conformations of the molecules being observed. These states can be detected and analyzed using Hidden Markov Modelling[12]. Hidden Markov Modelling is a statistical model that uses

observations of the data to reveal underlying probabilities. Before applying Hidden Markov Modelling, the general number of states observed should be estimated by the researcher based on the trace data collected. Hidden Markov Modelling is then applied using a program like HaMMY (developed by the lab of Dr. Taekjip Ha) to mathematically detect what FRET efficiency levels the various states observed are at, what the probability of transitioning between two states is, and what the probability is of starting in a particular state (Figure 4).

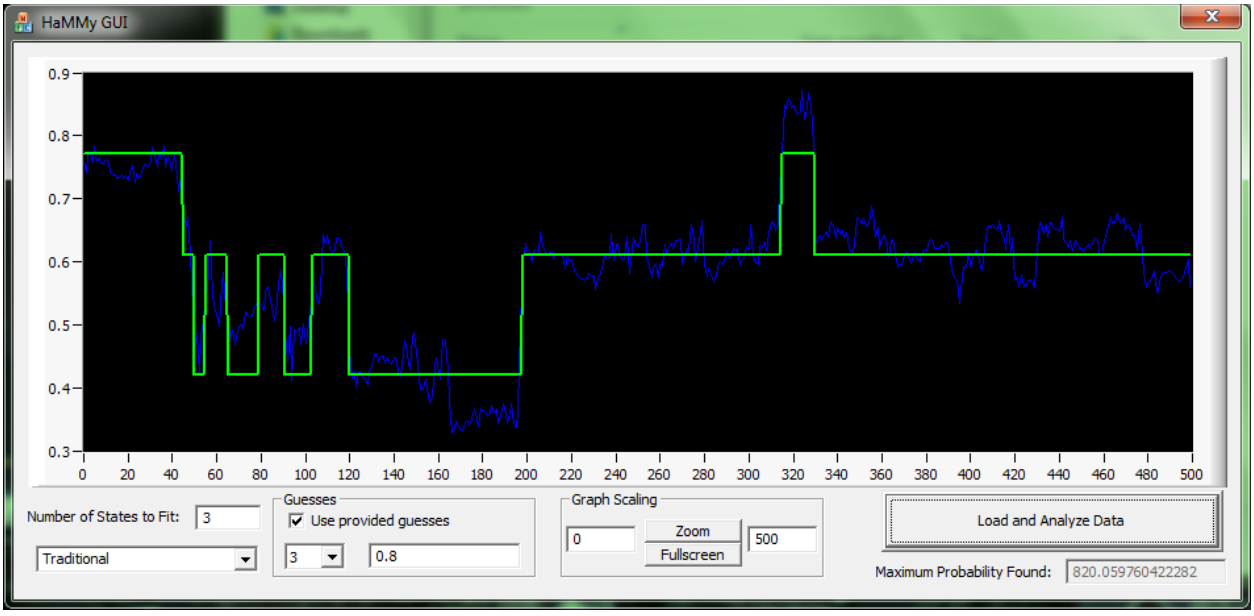

Figure 4. HaMMY. A screenshot of the program HaMMY applying hidden markov modelling to data from the peptide dimer CCL2-C based on starting estimates of three FRET states at .2, .6. and .8. Estimates are chosen based on previous CCL2-C data and user observations from trace data.

Human Immunodeficiency Virus

Human immunodeficiency virus 1 (HIV-1), an RNA lentivirus in the retroviridae family, is the infectious agent that leads to acquired immunodeficiency syndrome (AIDS)[13]. AIDS emerged among human populations in the early 1980s. Since the identification of the virus in 1983, HIV

has become a major epidemic around the world[14]. As of 2015, 36.7 million people around the world were living with HIV, with 2.1 million new HIV infections and 940,000-1.3 million HIV-related deaths occurring in 2015 alone[15]. Thanks to great developments in antiretroviral therapy and improved infection control, annual AIDS-related deaths have decreased by 28% since 2000, but much research remains to be done to further decrease the incidence of AIDS and AIDS-related mortality.

Initial infection with HIV leads to mild and non-specific symptoms including fever, rash, headache, or sore throat. Over time, HIV infection leads to a depletion in CD4+ T cells, which are the primary target of HIV-1. Viral load measured in viral RNA copies in the blood plasma during this time can range from <40 copies/ml to 100,000 copies/ml[16]. Progression to AIDS is defined as the point when the patient's CD4+ T cell count drops below 200 cells per µl of blood plasma[16]. At this point, the patient's immune system is severely compromised. As a result, opportunistic infections or malignancies that the immune system could otherwise effectively combat can take hold in the patient. These effects from the immune deficiency cause mortality in AIDS cases rather than the HIV virus itself.

Early treatment of HIV infection can drastically increase the patient's chance of survival and allow them to reach survival rates comparable to uninfected populations. For the vast majority of HIV-infected patients, successful treatment and suppression of HIV replication can be achieved through combination antiretroviral therapy (cART)[17]. cART uses a combination of retroviral drugs designed to target multiple HIV pathways simultaneously to block HIV replication and prevent HIV from being able to mutate resistance, as is it significantly more

difficult for the virus to develop resistance to multiple drugs at once than it is for HIV to develop resistance to a single specific drug. However, cART cannot completely eradicate the virus from the patient as HIV persists in memory T cells, where the provirus can remain transcriptionally silent and relatively un-targetable for years[18].

The HIV-1 virus consists of 2 strands of positive sense RNA packaged in the viral nucleocapsid complex. The nucleocapsid complex is further encapsidated by 1500 capsid protein monomers and the RNA and capsid are further wrapped in an envelope derived from the plasma membrane of the host cell the virus budded out of. The virus infects target cells when the virus glycoprotein, gp120, interacts with the cellular receptor protein CD4. Using CD4 and a co-receptor such as CCR5 or CXCR4, the viral envelope fuses with the host cell plasma membrane and releases the viral core into the cytoplasm (Figure 5A-C). The viral capsid must then traffic to the cell nucleus, uncoating along the way to release the viral RNA (Figure 5D). The viral RNA undergoes reverse transcription into a double stranded DNA product which translocates into the cell nucleus and integrates into the host cell genome through use of the viral integrase protein (Figure 5E). Once integrated into the host cell genome, the HIV genome becomes very difficult to accurately target and the virus can begin replication[16]. Understanding the early steps in infection is crucial to block HIV infection of target cells and for the development of antiviral targets.

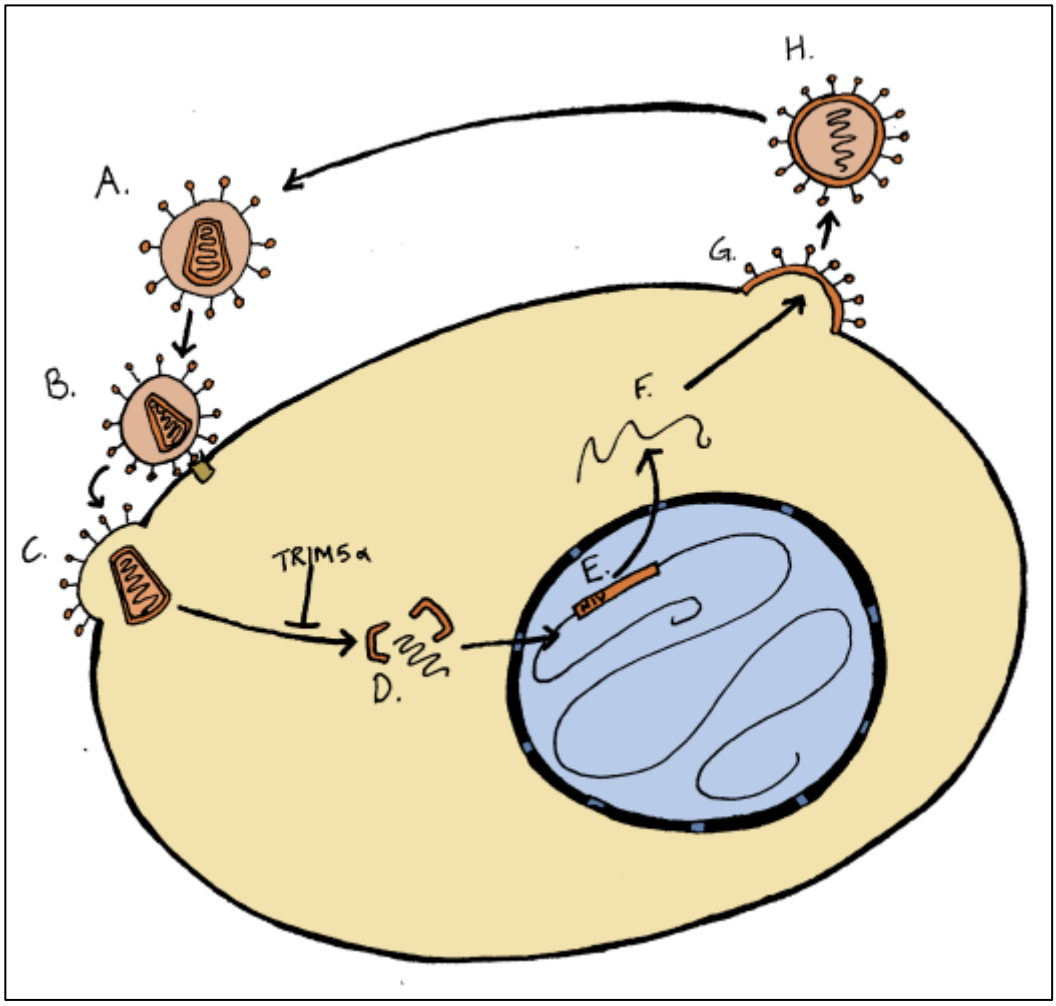

Figure 5. HIV Replication Cycle.
A: A mature HIV virus.
B: Attachment of the HIV viral glycoprotein to the cellular receptor protein CD4.
C: Fusion of the viral and cellular membranes and release of the viral core.
D: Dissociation of the viral core. Correct regulation of the uncoating process can be interrupted by the cellular protein TRIM5α.
E: Integration of the viral genome into the host genome.
F: Replication of the viral genome.
G: The virus budding from the host cell.
H: An immature free virion. The virion must undergo maturation before infecting a new cell.
Figure hand drawn by Margret Bradley

Tripartate Motif-Containing Proteins

Tripartate motif-containing proteins, or TRIM proteins, are interferon-inducible proteins involved in defense against various types of host pathogens[19–21]. TRIM proteins are characterized by three key domains: the RING (Really Interesting New Gene) domain, one or two B-box domains, and a long coiled-coil domain. The RING domain contains a zinc finger that can play roles in ubiquitination. After these three key regions, TRIM family proteins contain a number of different C-terminal domains which are thought to convey specific biological activity to these proteins.

TRIM5α.

TRIM5α was first discovered in 2004 to be capable of blocking HIV infection in rhesus macaques by Stremlau et al[22]. TRIM5α possesses only one B-box domain and has a SPRY domain following the coiled-coil helix (Figure 6A). TRIM5α typically exists as an antiparallel dimer[23]. In TRIM5α, the B-box domain is associated with the formation of high order TRIM structures as shown in (Figure 6C-D) [24–27]. The SPRY domain is associated with attachment to the HIV viral capsid[28–30]. While the complete TRIM5α protein is notoriously hard to purify, several sections of TRIM5α have been successfully purified for crystallography and other protein studies[27,31].

Rhesus TRIM5α is known to block viral infection of cells post viral entry. Interestingly, human TRIM5α does not effectively block HIV infection. Human TRIM5α does block infection from other lentiviruses, though, suggesting that human TRIM5α may have diverged from the

rhesus macaque version of the protein at some point to block a different viral threat to humans[32]. Interestingly, modification of a single amino acid in the SPRY domain of human TRIM5α to match the rhesus TRIM5α site does restore restriction of HIV by human TRIM5α suggesting that the human TRIM5α is defective in HIV capsid recognition[29,33]. Additionally, evidence has shown that, in high concentration such as that present in overexpression models or in the presence of stabilizing drugs, human TRIM5α does become a more potent inhibitor of HIV infection[34].

Possible Mechanism of Retroviral Restriction by rhTRIM5α.

The mechanism of retroviral restriction of TRIM5α is not yet fully understood. However, it is known that TRIM5α binds to the viral capsid and causes the premature disassembly of the HIV capsid[22,35]. Early studies by Stremlau et. al showed that TRIM5α accomplished dissociation of the HIV capsid without causing a reduction in capsid protein levels, showing that TRIM5α was not causing direct degradation of the capsid protein despite the hypothesis that the E3 ubiquitin ligase activity of the RING domain could lead to proteasomal degradation[36].

A second model of TRIM5α disassembly of viral capsid hypothesized that dissociation of the viral capsid occurred during proteasomal degradation of TRIM5α itself[37,38]. However, blocking the proteasome via MG132, a proteasome inhibitor, while it reduced restriction still resulted in inhibition of viral genome integration into the host genome[39–43]. Additionally, inhibition of the proteasome did not result in a buildup of TRIM5α, suggesting that TRIM5α degradation does not occur in a proteasome dependent manner[44].

Our current hypothesis is that TRIM5α, through dynamic conformational changes in the Linker 2 (L2) region that folds back across the coiled-coil domain and links the coiled-coil to the SPRY domain causes strain on the viral capsid[45,46]. If the conformational changes in the L2 region are great enough, then TRIM5α may be able to independently physically pull the HIV capsid apart via torsional strain.

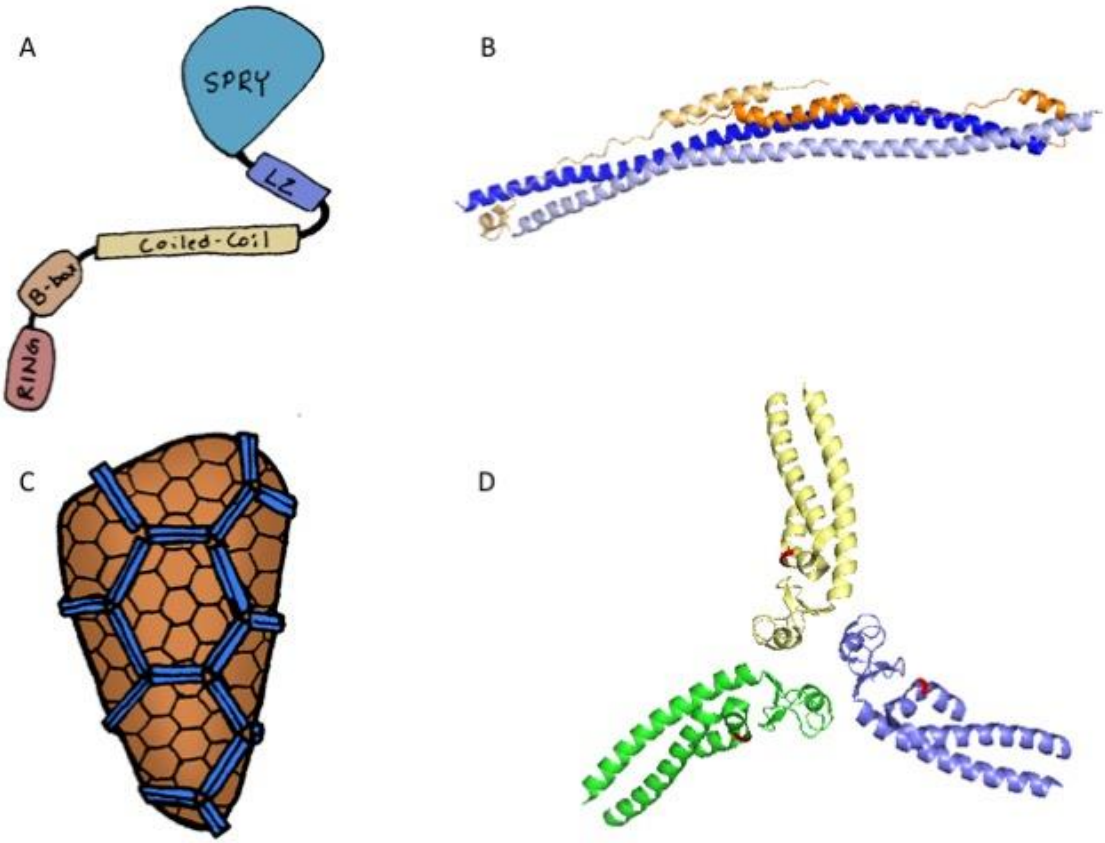

Figure 6. TRIM5α Structure and Mechanism.
A: Diagram of the domains of TRIM5α.
B: Modelled structure of the coiled coil and linker 2 (CCL2) domains of TRIM5α as used in this thesis. The structure shown is a dimer with the coiled-coil domains in blue and the linker 2 domains in orange. Based on the crystal structure determined by Goldstone, et al. (2014)
C: Diagram of a TRIM5α cage around an HIV capsid. TRIM5α is depicted in blue while HIV capsid is depicted in orange.
D: Structure of the B-Box mediated trimerization of TRIM5α proteins as determined by Wagner, et al. (2016)
Panels A and C hand drawn by Margret Bradley

CHAPTER II: MATERIALS AND EXPERIMENTAL METHODS

Recombinant DNA Constructs

Constructs of the coiled-coil and linker 2 (CCL2) domains of Trim5α were amplified with PCR using full length Trim5α as a template and Phusion High-Fidelity PCR Master Mix (Thermo Scientific). The PCR products were then cloned into a pET-15b protein expression vector using the restriction enzymes NdeI and BamHI. The pET-15b protein expression vector contains an N-terminal His-tag with a thrombin site, the lac promoter, and an ampicillin resistance cassette.

Ligated plasmids were transformed into NEB 5-alpha competent, high efficiency *E.coli* cells and the plasmids were analyzed after miniprep by diagnostic digest using the restriction enzymes used to clone into the vector and running the final product on a 1% agarose gel with ethidium bromide. If the diagnostic digest produced bands of the correct size on the agarose gel, samples were sent for sequencing at the University of Chicago Center for Genomic Research.

Protein Induction and Purification

For protein induction and purification, BL-21 *E.coli* cells transformed with pET-15B plasmids containing the desired His-tagged protein sequence were grown in 5 ml overnight LB +carbenicillin cultures from either picking a colony off of a fresh LB +ampicillin plate or from frozen glycerol stocks of BL-21 bacteria containing the plasmid kept at -80°C. The next morning,

1-5ml of the overnight cultures were added to 250ml LB +carbenicillin and shaken at 37°C for 2-4 hours or until the bacterial cultures reached a density with OD of 0.6-0.8. The cultures were then induced by the addition of IPTG to 1 uM and shaken at 37°C for 4 hours. After induction, the cultures were spun down at 5400rpm in a Sorvall RC 6+ centrifuge for 20min. The supernatant was discarded and the pellet was frozen at -20°C for storage until purification.

When ready for purification, the pellet was thawed on ice and vortexed to break up the pellet. The pellet was then resuspended in 4ml Lysis buffer (50mM Sodium Phosphate buffer pH8, 500mM NaCl, 8M Urea, .5mg/ml lysozyme, 1% Triton X, 10 mM imidazole, and EDTA-free protease inhibitor cocktail) and sonicated for 1 minute in 10 second bursts. The sonicated cells were spun in a Beckman Coulter Optima L-90K ultracentrifuge at 10K rpm for 30min. The supernatant was combined with TALON Metal Affinity Resin Beads (Clontech) that had been equilibrated in 50mM Sodium Phosphate pH8, 500mM NaCl, 8M Urea buffer and mixed at 4°C for 1 hour. The pellet from ultracentrifugation was normally discarded. After mixing, the supernatant and beads were applied to a Clontech disposable gravity column and washed several times with 50mM Sodium Phosphate pH8, 500mM NaCl, 8M Urea buffer. The proteins were eluted by adding imidazole to 150 mM in either leftover lysis buffer or wash buffer and adding 1 ml elution buffer to the capped column. The column was left to sit in elution buffer for 15 minutes at 4°C before collection in microcentrifuge tubes. For each protein, elution was repeated 3 times. Eluted protein could then be checked via western blot or coomassie stain for proper production and stored at -20°C.

To prepare proteins for use and analysis, they were dialyzed in decreasing concentrations of Urea (4M, 2M, and 0M Urea in 50mM sodium phosphate 500mM NaCl pH8 buffer) with at least 3 hours per step or overnight. Dialysis was performed using 1-3 ml 10,000 MWCO Slide-A-Lyzer dialysis cassettes (Thermo Scientific). Final protein concentrations were obtained using a Thermo Scientific Nanodrop 2000.

Protein Analysis

Purified proteins were analyzed by loading the proteins onto 12% polyacrylamide gels. Loading dye was chosen based on whether we were looking for the protein in monomeric or multimeric forms. For monomeric protein, we used 2x SDS glycerol dye with 1 µl β-mercaptoethanol. For multimeric protein, we used 2x SDS glycerol dye without β-mercaptoethanol. Proteins were incubated with dye at 100°C for 5 minutes and briefly cooled on ice before loading. Two main methods for protein detection were used. For rough analysis of sample purity and protein concentration, the gels were coomassie stained with Imperial dye (source) for one hour at room temperature and washed in DI water for one hour or overnight for better resolution. Finished coomassie gels were imaged using a Proteinsimple imager.

For more sensitive assays detecting lower protein concentrations we used western blotting to detect His-tagged proteins. After protein separation, proteins were transferred onto a nitrocellulose membrane and detected using an anti-Histidine antibody conjugated to horseradish peroxidase (αHis-HRP) (Santa Cruz Biotechnology). The membrane was imaged using chemiluminescent substrate and a Proteinsimple imager.

Circular Dichroism

Circular dichroism was performed on CCL2 proteins at the University of Illinois-Chicago Protein Research Laboratory (PRL) on their Jasco 710 spectrophotometer with the help of Bob Lee, the PRL director. Proteins were dialyzed further into low salt buffer to decrease the effect of salt on resultant CD measurements (50mM sodium phosphate 150 mM NaCl pH8 buffer) and diluted to 50µg of protein in 600µl buffer before shipping to the University of Illinois-Chicago on dry ice. Use of Tris or sodium phosphate buffers at the same pH and salt concentrations did not appear to make a difference in circular dichroism readout. Circular dichroism analysis was carried out at room temperature (25°C) and data were returned to us in molar ellipticity units in Excel files accounting for protein concentration, residue number, and dimerization.

Percent secondary structure content of each protein was calculated using CDpro (http://sites.bmb.colostate.edu/sreeram/CDPro/). Data were first entered into CRDATA which converted the molar ellipticity units into molar absorbance (Δε) units and generated an INPUT file which can be read by any of the 3 analysis programs included in CDpro. We then used SELCON3 along with reference set 10 provided as part of the CDpro software to calculate secondary structure of the protein from the circular dichroism data.

Protein Labelling

Before protein labelling, cysteine-tagged proteins were dialyzed into phosphate buffer at pH7 to prevent interference of higher pH with the maleimide to cysteine conjugation reaction. Dialyzed proteins were then incubated with Tris(2-carboxyethyl)phosphine (TCEP) at 4°C overnight to break up disulfide bonds existing in the proteins. TCEP does not interfere with

the maleimide conjugation reaction and does not need to be dialyzed away before beginning labelling.

Alexa 488 and Alexa 594 maleimide conjugated fluorescent dyes were ordered from Invitrogen, resuspended in anhydrous dimethyl sulphoxide (DMSO), and stored at -20°C. To label cysteine-tagged proteins, a 3-fold molar excess of maleimide dye was added to the protein and the solution was incubated at room temperature for 45 minutes or overnight at 4°C before the reaction was halted by the addition of β-mercaptoethanol. Dye was then removed using .1-.5 ml 10,000 MWCO Slide-A-Lyzer dialysis cassettes (Thermo Scientific) over the couse of several dialysis steps performed at 4°C. To dual label dimers of CCL2-C, Alexa 488 and Alexa 594 dyes were added simultaneously at a 1:1 ratio.

Single-Molecule Förster Resonance Energy Transfer (smFRET)

Slide Surface Preparation for smFRET.

For Single-Molecule Förster Resonance Energy Transfer (smFRET) analysis, slides first need to be thoroughly cleaned to remove any old sample or contaminants and coated so the sample molecules can adhere to the surface of the slide. Our slides, both quartz and glass, were drilled with beveled holes at the ends of the area a coverslip would cover. The beveling of the holes allows for moderate pressure to be applied when loading assembled microfluidic chambers and eliminates need for tubing to load samples. The following cleaning method was initially developed by the Miller Lab.

Slides were first soaked for 24+ hours in 10% Contrad solution to remove old tape, sealant, and any marker notations. Any old tape, coverslips, and other waste was discarded in containers marked for sharps and glass disposal. Slides were rinsed in water and placed in a Teflon slide holder built for the lab. The slides were covered in water and boiled on a hot plate for 20 minutes to remove any remaining residues. Next, slides were sonicated for 40 minutes in 10% Contrad solution, rinsed, and sonicated for 40 minutes in water using a Branson bath sonicator.

Coverslips were loaded into a Teflon coverslip holder similar to the slide holder and included in the procedure from this point onwards. Slides and coverslips were rinsed with water, sonicated in 1M potassium hydroxide (KOH) for 20 min to etch the glass surface, and rinsed again in water. They were then rinsed with methanol, sonicated in methanol for 40 minutes, rinsed with water and sonicated in water for 10 minutes. At this stage, slides and coverslips were dried with nitrogen gas to prevent oxidization. The slides and coverslips were then sonicated in methanol for another 5 minutes.

To activate the glass surface, the slides and coverslips were incubated in 1% 3-aminopropyltriethoxysinane (APTES) reaction solution (100 ml methanol, 5 ml acetic acid, 1 ml room temperature APTES). Slides and coverslips were incubated at room temperature for 10 minutes in the APTES solution, sonicated for 1 minute, and incubated for another 10 minutes. The slides and coverslips were then rinsed first with methanol, then with water, then again with methanol before drying with nitrogen gas.

The final slide preparation stage applies a PEGylation layer to the slides and coverslips. A fraction of the PEG molecules are conjugated to a biotin tag that later sample reagents can adhere to. Fresh PEGylation buffer was prepared for each batch of slides and coverslips coated (84mg sodium bicarbonate in 10ml MQ-water). 80 mg m-PEG (polyethylene glycol) and 5-8 mg biotin-PEG equilibrated at room temperature were weighed out and dissolved in 320 µl PEGylation buffer. The PEG solution was briefly vortexed to mix and centrifuged to remove bubbles. Fresh PEG solution was made for each 5 slides coated. Slides were placed with the side to be coated facing up in humidification chambers constructed from 1 ml pipetter tip boxes with wet Kim-wipes or paper towels placed in the bottom section. 70 µl of PEGylation reaction solution was placed on top of the slides between the holes drilled for microfluidic chamber loading. Once any bubbles dissipated, a coverslip was carefully dropped on top of the PEGylation reaction solution and gently adjusted to remove any accidentally introduced bubbles. Slides and coverslips were marked with an arrow in the top left corners for easy identification of the PEGylated surface later on and incubated in the dark overnight at room temperature (no more than 16 hours). After incubation, the slides and coverslips were carefully separated, rinsed with MQ-water, and thoroughly dried with nitrogen gas in 50 ml conical tubes. The tubes containing the slides were sealed with parafilm and stored at -20°C until the slides were ready for use.

Microfluidic Chamber Preparation for smFRET.

To construct the microfluidic chamber for smFRET, cleaned and PEGylated slides and coverslips were taped together with double-sided scotch tape long enough to reach slightly

past both ends of the coverslip with a gap of a centimeter or less between the two strips of tape. The coverslip was placed so that the coverslip covered both of the holes drilled in the slide and the tape did not block the holes in the slide. This creates a microfluidic chamber no more than a millimeter in depth. The ends of the microfluidic chamber may be sealed with grease or epoxy, but epoxy creates a mess easily and grease does not hold well in response to any pressure in the chamber. Sealing the chamber by carefully applying hot wax to the ends using a large needle attached to a stick as a scoop worked very well. The assembled chamber should look as shown in Figure 7.

Once the wax cooled, we prepared to load the chambers. Fresh imaging buffer was made (20 mM Hepes/Tris-Cl, 150 mM NaCl, 0.1 mg/ml BSA, 2 mM Trolox) each day we did smFRET. A stock of 100 mM propyl gallate was prepared in ethanol beforehand and stored in 100 µl aliquots at -80°C. The microfluidic chamber was first loaded and incubated with 50 µl of 0.2 ml/ml neutravidin in imaging buffer for 5 minutes. After a wash with 100 µl imaging buffer, the chamber was loaded with 70 µl 10 nM penta-his biotin-conjugated antibody (Qiagen) in imaging buffer and incubated for 10 minutes. After a third wash with 100 µl imaging buffer, the chambers were loaded with 90 µl 1nM labelled sample protein mixed with propyl gallate added to 1 mM. The sample was incubated in the chamber for 20 minutes in the dark and flushed with 100 µl imaging buffer before imaging. If the chambers would not be imaged shortly after they were made, the chambers were stored in a Styrofoam box containing small amounts of ice.

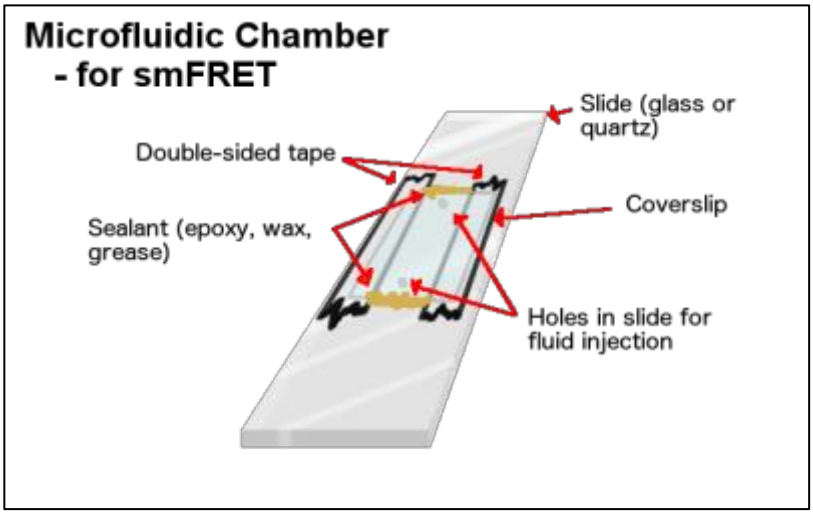

Figure 7. Microfluidic Chamber Construction. Microfluidic chambers are constructed using highly cleaned quartz or glass slides and coverslips that are assembled using double-sided tape and sealed using epoxy, wax, or grease. Figure drawn by Margret Bradley using the program GIMP.

smFRET Using Objective TIRF.

smFRET using objective total internal reflection fluorescence (TIRF) microscopy was developed for the Campbell Lab at Loyola University Chicago with the use of a TIRF microscope belonging to the lab of Dr. Seth Robia. The microscope was fitted with a Optosplit II Image Splitter from Cairn Research and a custom ordered splitter filter cube (ET 535/70, ET 645/75, T600lpxr-UF2=400, UF1=300). The laser on the microscope was set to 488nm for excitation of Alexa 488 using filters and no other filters were used on the excitation laser. Prior to collecting any data, images were taken of a calibration slide using minimally cleaned, undrilled slides and coverslips to create a completely sealed microfluidic chamber containing 0.2µm orange (540/560) FluoSheres Fluorescent Microspheres (Invitrogen). All data were obtained from microfluidic chambers where the glass coverslip was facing downwards towards an 100x oil

immersion objective. Image focus was maintained throughout data acquisition using the perfect focus system on the microscope.

Data were collected on both calibration bead slides and sample slides using the program Single developed by the lab of Dr. Taekjip Ha (available open source on the lab website). Simple must be run in administrative mode and cannot control filters on the microscope but is used to control the camera and adjust rotation of the image. As data files for smFRET can be very large (typically between 8-30GB of data produced per run) data were recorded on the computer associated with the microscope and transferred to an external hard drive for backup and transport to other computers for analysis.

smFRET Data Mapping.

Data analysis for smFRET data takes several stages to produce a final product. Programs for data analysis were developed by the lab of Dr. Taekjip Ha. Immediately post acquisition, data were mapped and converted to .trace files which could be read by the Matlab programs using IDL. A mapping file to generate a coordinate map to match molecules in the left and right acquisition windows created by the splitter was first generated from the images taken of the beads slides. Generating the mapping file involves running data sequentially through the IDL programs Maketiff, Calc_mapping2, and Nxgn1_cm. For each program, the correct file path for the beads files can be set by manually modifying the program code. All active IDL programs were re-compiled each time a file path modification was made. Maketiff first converts the collected data into a file IDL can work with more easily. Calc_mapping2 allows the user to choose matching three points from the left and right windows of the image and align the

program (Figure 8A-B). Nxgm1_cm detects all peaks of light in the image and attempts to match all peaks on the left to peaks on the right (Figure 8C). Nxgm1_cm will also output both how many peaks were found and how many successful pairs were mapped. By multiplying the pair count by 2 and dividing by the total number of peaks, a quantitative quality of the mapping file can be determined. The higher the percent of mapped pairs in the file, the better the quality of the file. Ideally, about 90% of the peaks or more should be matched to a pair.

Once a mapping file of acceptable quality has been generated, the sample data can be mapped as a batch using the IDL programs Ana_all, P_nxgn1_ap, and P_nxgn1_ffp. Manually set the file path in P_nxgn_ffp to the chosen beads file and set the file path in Ana_all to a folder containing subfolders of data. If the folder structure for Ana_all is incorrect (e.g. leading directly to a folder containing data), the program will produce an error message. Once the correct file paths are set in the programs, simply running Ana_all will begin the analysis of all the data.

A

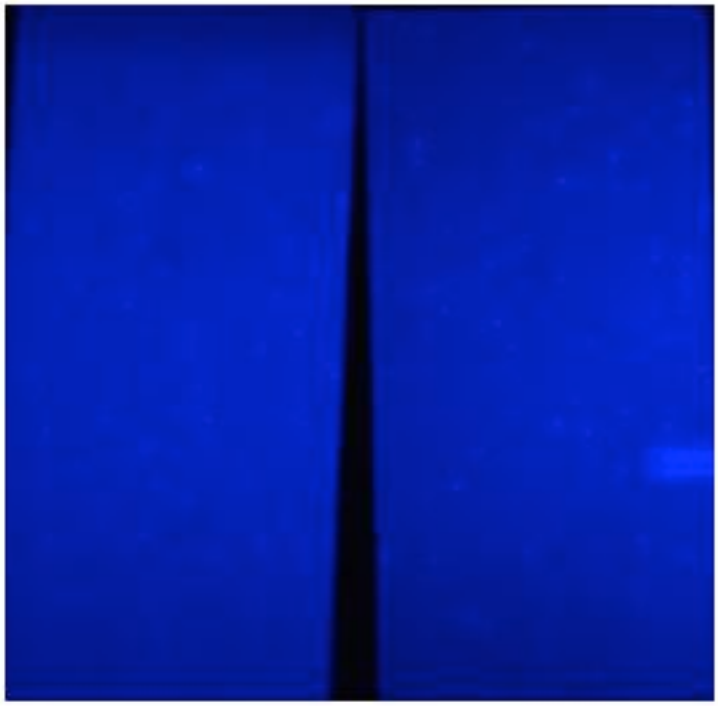

B

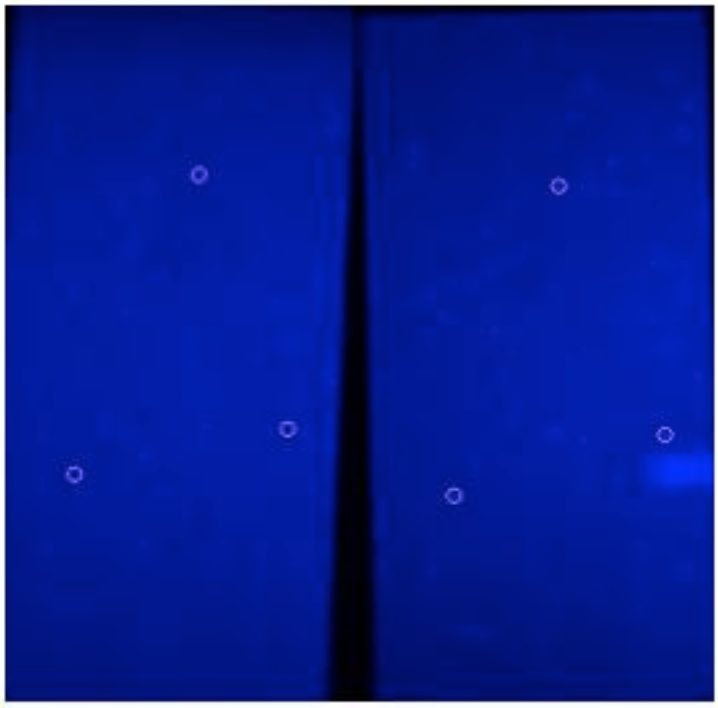

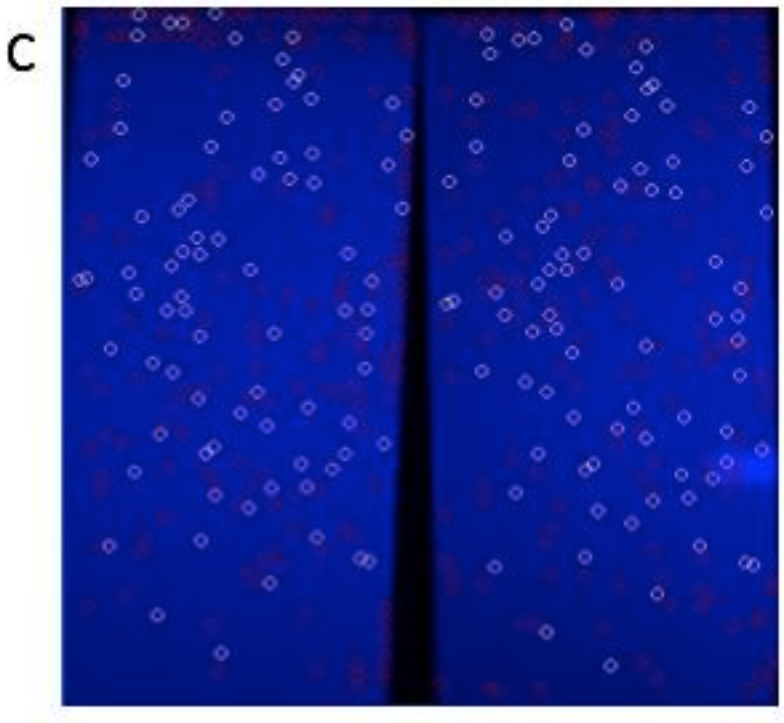

Figure 8. Creation of a Mapping File in IDL.
A: The raw image compiled from a smFRET bead file calibration movie. Note the visible bright points corresponding to the beads. (Maketiff program)
B: Selection of three points in a triangle around the sample on the left and right. This is done by hand and is pest done with the three points spread out to provide better coordinates. (Calc_mapping2 program)
C: Software detection of the remaining correlating peaks in the beads file. (Nxgn1_cm program)

smFRET Data Analysis.

Once the data have been mapped and converted to trace files using IDL, analysis of individual traces and compiled data could be performed in Matlab using TirfLite 2.0, a program package developed by Raymond Pauszek in the lab of Dr. David Millar of the Scripps Research Institute. Traces were first selected for quality in the tirf_movieprocessing subprogram. A high quality trace shows at least one or two FRET transitions, a high anticorrelation coefficient wherein the individual fluorophore traces behave in an opposite manner, a single-step

photobleaching, and baseline fluorophore intensity after the photobleach step. Flashes of fluorophore intensity may be observed after the photobleaching step, but are disregarded as the trace is cropped after the photobleach. Bleedthrough of the donor (488) fluorophore into the acceptor (594) channel can also be calculated using sample labelled only with the Alexa 488 fluorophore. While selecting traces, non-linear smoothing was applied to the traces for ease of use in distinguishing transition events. Smoothing, however, can oversimplify data and alter how it appears in later steps so selected traces were exported and saved as unsmoothed data.

The .mat files of the traces from the previous step were next combined into a single folder, either manually or using the combinemoviefolders helper script in Matlab. The TirfLite subprogram, vfit, was then used to reexamine the traces selected in tirf_movieprocessing. Any traces deemed to be of suboptimal quality were filtered out of the data set. In vfit, the selected data also output a histogram to which curves outlining the expected stable states could be fit. The program calculates the probability of the dimer being in a specific FRET conformation and the probability of transition between different FRET conformations as well as providing an initial estimate for Hidden Markov Modelling (HMM) of the FRET states using viterbii fitting. Once the traces had been trimmed and filtered, they were exported for analysis in HaMMY, a software package developed by the lab of Dr. Taekjip Ha available open source on the lab website. HaMMY fits selected FRET states to the FRET trace data and maps transitions using Hidden Markov Modelling and outputting files in a .hmm file format.

Finalized HaMMY files are loaded into viewhammy2, a TirfLite 2.0 subprogram which then compiles the HaMMY data into a TDP plot which show a heat map of the different FRET states and the probability of transition between states.

Optosplit Calibration.

During the course of use, the Optosplitter used for splitting the emission wavelengths of smFRET can come out of calibration which can cause downstream problems in data analysis, namely because the IDL program used to create initial mapping files of the data is extremely finicky if the image isn't split exactly in half or has too few bright peaks. Therefore, the Optosplitter must occasionally be calibrated. Poorly done calibration can make the situation infinitely worse, so careful reading of the Optosplit manual is recommended. For calibration of a splitter that has come extremely out of alignment, however, additional steps not listed in the manual must be taken.

If calibration of the cube does not seem to correct using the calibration instructions in the manual, remove the splitter cube so that only a single channel is visible in brightfield illumination. Narrow the aperture using the sliding tabs near the microscope end of the Optosplit box so that all sides of the opening are visible in Single. Next move the channel to the center using the V2 (vertical) and split control (horizontal). Once the channel is in the center, re-insert a cube and align the two channels so that they are superimposed using the V1 vertical knob and a combination of the horizontal (H2) and split controls to keep the superimposed images in the center. These steps may need to be repeated several times depending on how

out of calibration the Optosplitter has gotten. Finally, reduce the width of the aperture and split the two channels using the split control knob so that you see two channels side by side.

CHAPTER III: RESULTS

Generation of Recombinant, Fluorophore-Conjugated Protein Suitable for Single-Molecule FRET

Purify CCL2 Peptides with Cysteines to Allow for Fluorophore Labelling.

To generate a peptide for fluorophore labelling from TRIM5α, we first isolated the Coiled-Coil and Linker 2 domains of TRIM5α. The Linker 2 region has previously been shown to have dynamic regions by crystal structure which may correlate to spring-like flexibility down the more stable Coiled-Coil helix (Figure 9)[31,46]. The SPRY, RING, and BBox domains were excluded both to simplify the system and due to difficulty in purification. Because there were no native cysteines in the Coiled-Coil or Linker2 domains, we were able to introduce cysteines in positions we chose and take advantage of maleimide chemistry to link maleimide-tagged fluorophores to the thiol of the cysteine residue to achieve site-specific labelling on the peptide[5]. For single molecule FRET, we choose to place the cysteine at the C-terminal end of the peptide, which is the end of the Linker 2 domain.

After cloning into the pET-15b plasmid vector, which is designed for protein purification, we confirmed both that the CC and L2 domains were intact and that the C-terminal cysteine was present via sequencing. Since the TRIM5α dimer is fairly soluble, the peptide, which we named CCL2-C, did not require extraction from the pellet of bacterial debris during purification.

Sonication in lysis buffer followed by ultracentifugation was sufficient to release the CCL2-C protein from the E. coli cells (Figure 10). To attempt to get the peptides back into their native conformation post purification, we used dialysis to remove urea from the protein buffer.

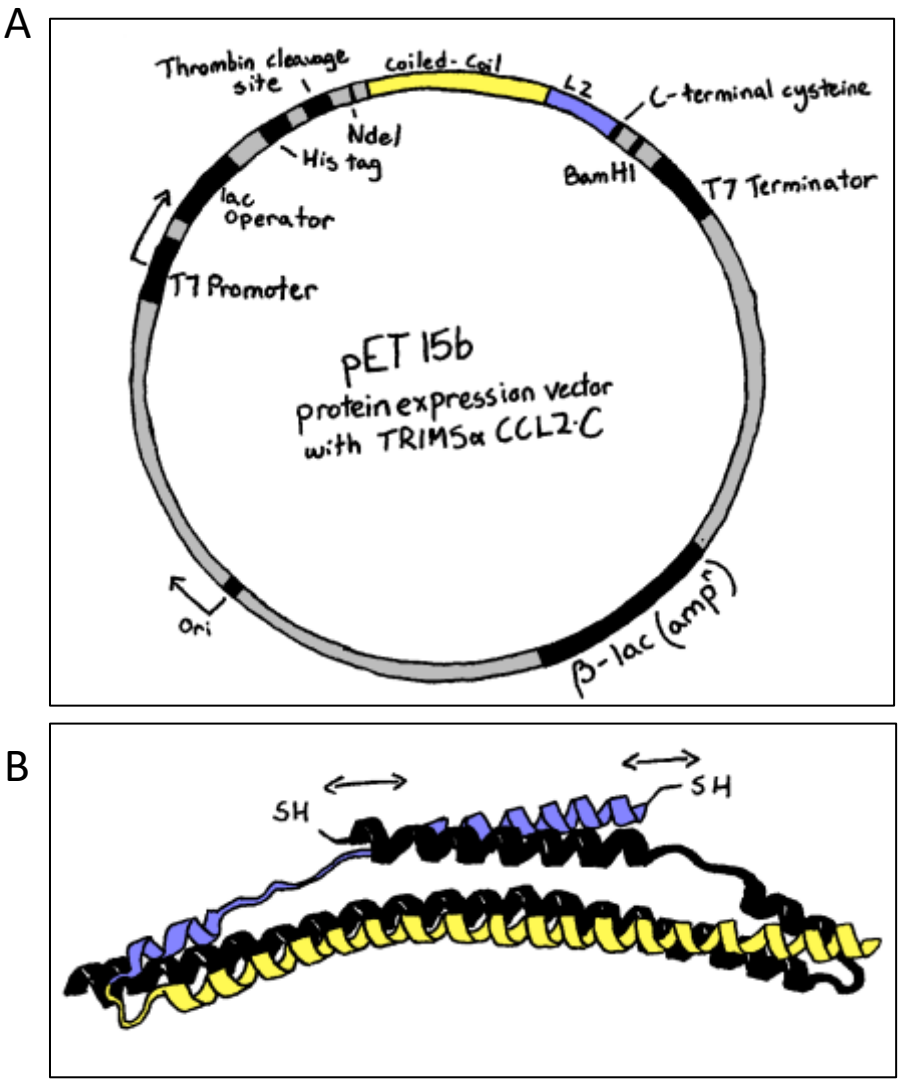

Figure 9. Design of CCL2-C for Protein Purification.
A: Diagram of the pET-15b vector for purification of the CCL2-C protein. Important plasmid features include ampicillin resistance and a His-tag for protein purification.
B: The proposed molecular model of a CCL2-C dimer. One subunit of the dimer is entirely in black. On the other dimer subunit, the Coiled-coil (CC) domain is shown in yellow and the Linker-2 (L2) domain is shown in purple.
Figure hand drawn by Margret Bradley.

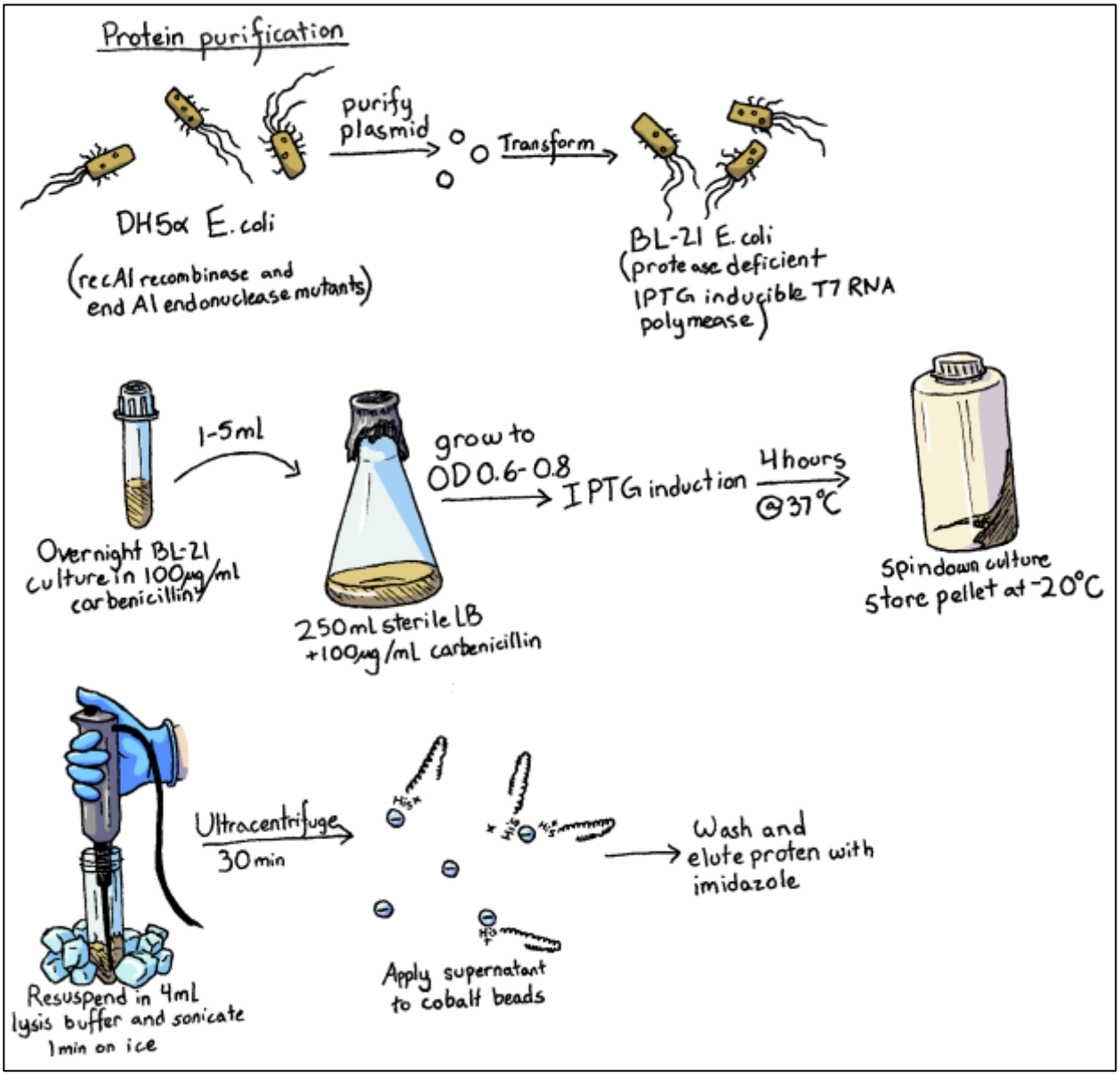

Figure 10. Protein Purification Protocol. Pictorial representation of the method for purification of the CCL2-C protein. Figure hand drawn by Margret Bradley.

Design a Method to Efficiently Label CCL2-C with Fluorophores that can Produce FRET Without Disrupting the Secondary Structure of the Protein.

For single-molecule FRET analysis, proteins must be labelled with fluorophores that are small to prevent disruption of secondary structures and increase specificity[1]. The fluorophores must also have overlapping excitation and emission wavelengths so that FRET can occur. For our experiments, we chose Alexa 488 and Alexa 594 as our donor and acceptor, respectively, which FRET with an R_0 of 60Å, meaning FRET is 50% efficient when the fluorophores are 60Å apart (Figure 11A-D)[47]. We used maleimide conjugation to link the CCL2-C proteins to maleimide derivatives of the Alexa 488 and 594 fluorophores (Figure 11E). The proteins first needed to be dialyzed into a pH7 buffer to optimize the maleimide chemistry before they are combined with commercial dyes re-suspended in DMSO.

We tried two different labelling methods for CCL2-C. The first method involves labelling CCL2-C in separate batches of Alexa 488 and Alexa 594. The labelled proteins are then denatured using 8M urea. The separately labelled proteins are combined while denatured and dialyzed over the course of several days into buffer without urea to allow the proteins to fold back into their native shape. While we have achieved smFRET using proteins labelled this way, the labelling process is both long and runs the risk of permanently denaturing the proteins.

To avoid potential pitfalls of our initial labelling method, we attempted to label the proteins using both dyes at once. Our hypothesis was that the proteins would be labelled one quarter Alexa 488 dimers, one quarter Alexa 594 dimers, and one half dimers with both Alexa 488 and 594. Theoretically, the ratios should be similar to those seen when the proteins are

denatured and combined after labelling. We found that we were indeed able to observe FRET using a method combining both dyes at once.

In summary, we developed a method that does not require denaturing the proteins to combine the two fluorophores and found that we could still observe smFRET in the proteins after excess dye had been removed.

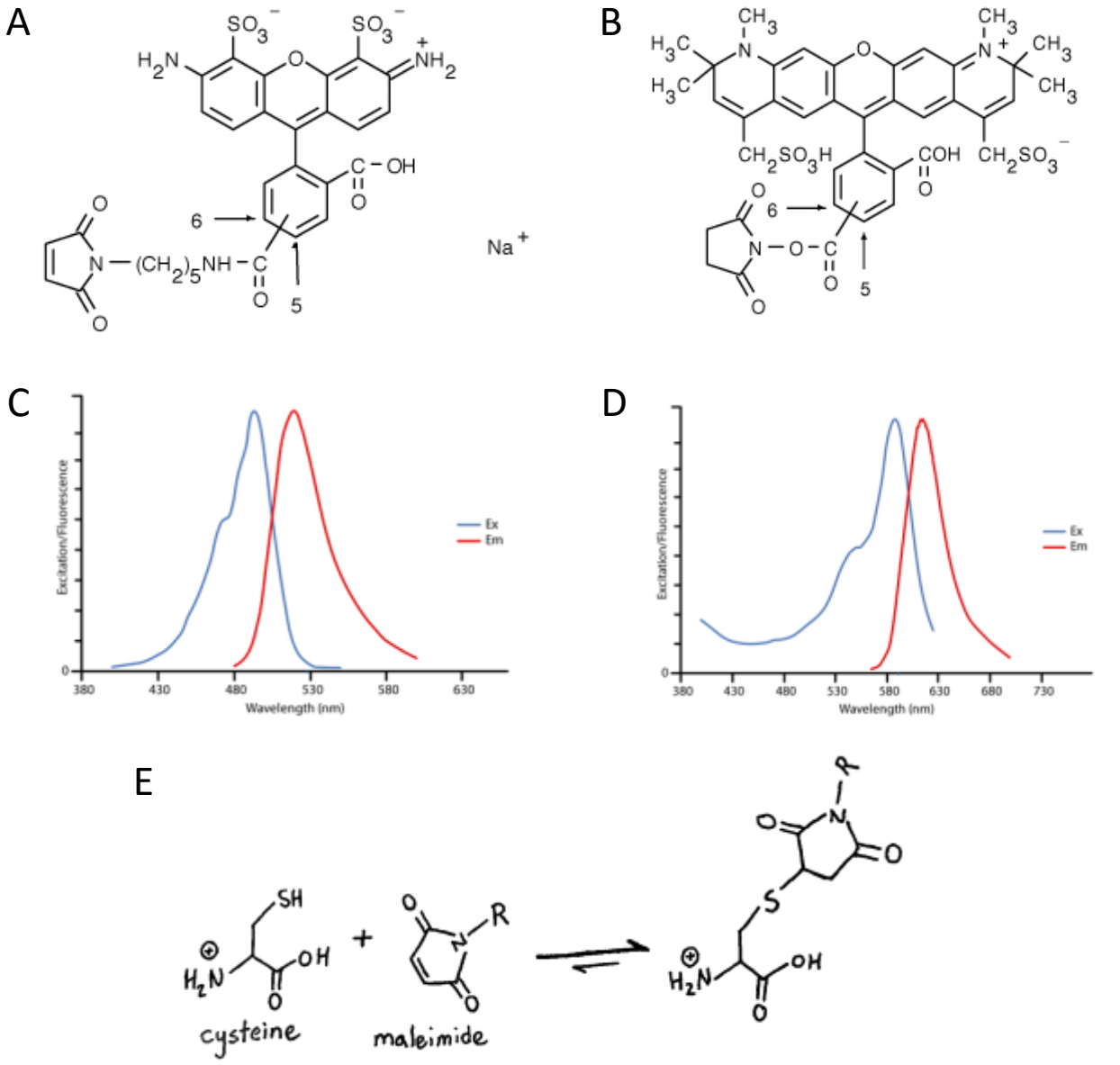

Figure 11. The Alexa 488 and Alexa 594 Fluorophores.
A: Maleimide conjugated Alexa 488 molecular structure.
B: Maleimide conjugated Alexa 594 molecular structure.
C: Excitation and emission spectra for Alexa 488.
D: Excitation and emission spectra for Alexa 594.
E: Maleimide-cysteine conjugation reaction.
Molecular structures and spectra obtained from the Thermo Fisher product website. Alexa 488: https://www.thermofisher.com/order/catalog/product/A10254. Alexa 594: https://www.thermofisher.com/order/catalog/product/A10256. Maleimide conjugation Reaction hand drawn by Margret Bradley.

Characterize the Purified and Labelled Proteins via Western Blotting and Circular Dichroism.

To characterize the purified proteins, we primarily used western blot. Since freshly purified CCL2-C will naturally make a stable dimer due to disulfide bonds that can be disrupted with a denaturing agent such as β-mercaptoethanol, we could use a combination of denaturing and non-denaturing acrylamide gels to determine both how pure a fresh protein purification was and whether the protein was generally behaving as expected. While we typically used coomassie gels, we also used western blots against the 6-His tag on the proteins for greater sensitivity. Denaturing gels show a single heavy band at 22kDa while non-denaturing gels run without β-mercaptoethanol show both the 22kDa monomer band in addition to an approximately 44kDa dimeric band (Figure 12A-B). We also found that more sensitive western blot gels also occasionally showed higher molecular weight bands potentially representing higher order aggregates of CCL2-C.

Characterization of protein labelling was done via typhoon imaging which takes fluorescent images of fluorescently-tagged proteins run on a standard acrylamide protein gel. We found that successfully labelled proteins were detected in both the 610 and 523 emission detection channels corresponding to the Alexa 594 and 488 fluorophores (Figure 12C-E)[45].

Further characterization of the protein secondary structure was done using circular dichroism[48]. We found that purified CCL2-C had a very similar secondary structure to CCL2 without the C-terminal cysteine and that the secondary structure percentages were close to those predicted by published crystal structures of CCL2 (Figure 13B). Additionally, while buffer

can potentially affect secondary structure and detection by circular dichroism spectropolarimeters, keeping CCL2 in phosphate or TRIS buffers did not appear to affect secondary structure (Figure 13A and C)[48].

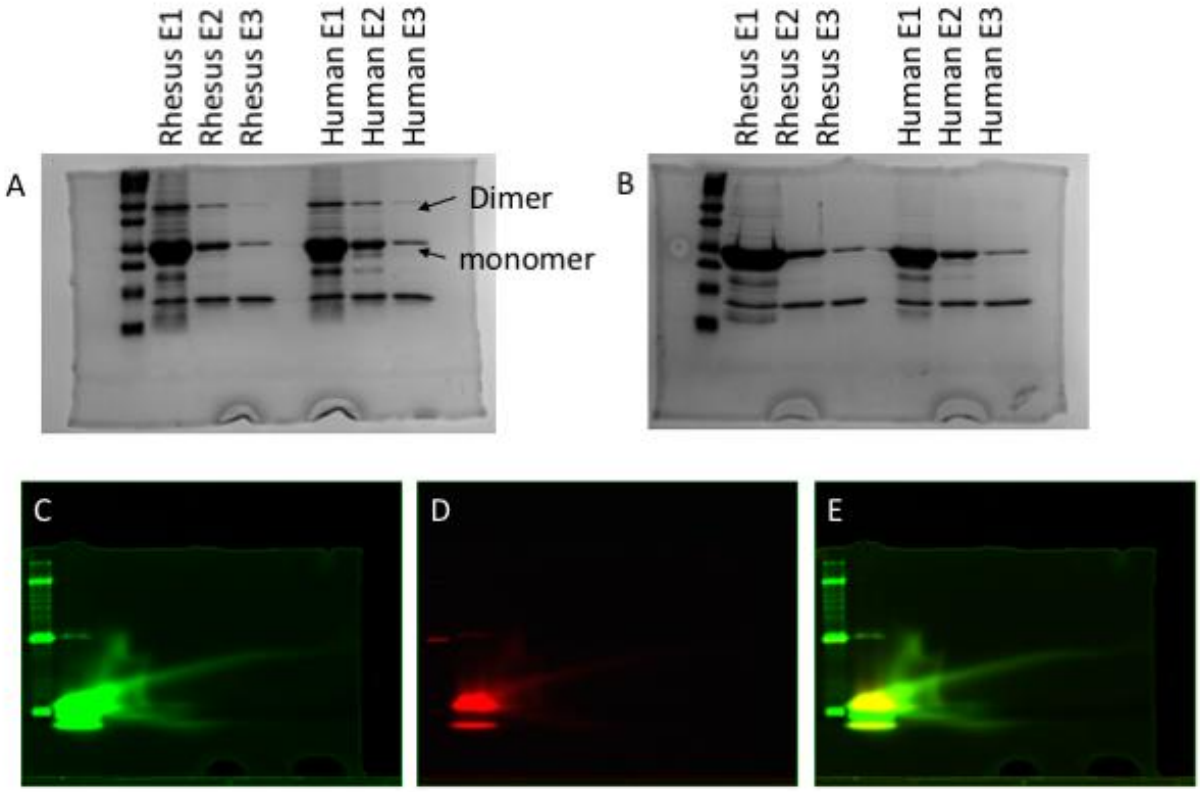

Figure 12. Protein Gel Analysis of CCL2C.
A: Unreduced protein purification acrylamide gel with three elutions each of Rhesus and Human CCL2-C showing the monomer and dimer bands. The lower band is junk protein that is removed via subsequent dialysis.
B: Reduced (+βME) protein purification acrylamide gel with three elutions each of Rhesus and Human CCL2-C showing only the monomeric band.
Typhoon image of labelled human CCL2-C showing the C: Alexa 594 emission, D: Alexa 488 emission, and E: merge.

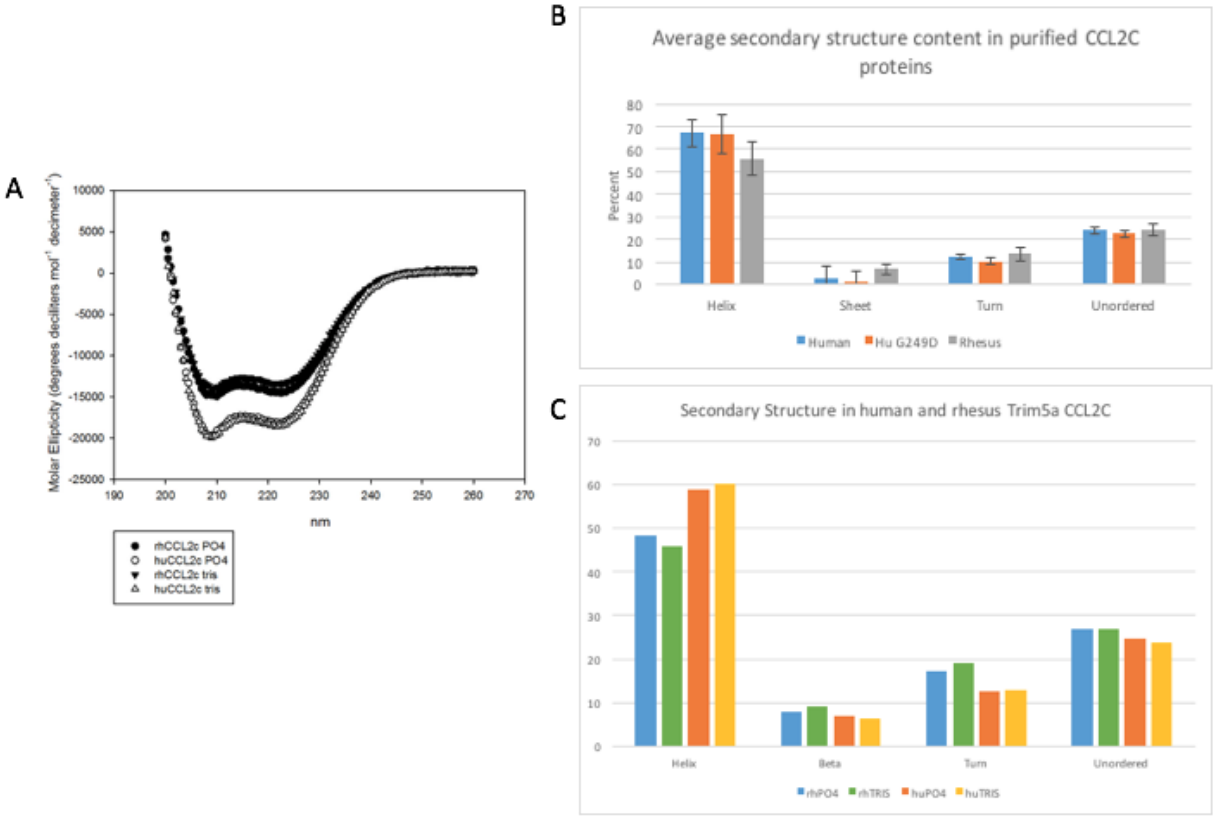

Figure 13. Circular Dichroism Analysis of CCL2-C.
A: Circular dichroism spectra of human and rhesus CCL2-C in phosphate and TRIS buffers run in duplicate.
B: Percent secondary structures detected in CCL2-C proteins derived from human, rhesus, and a G249D mutant of human TRIM5α. Data were averaged from three replicates.
C: Secondary structure detected in human and rhesus CCL2-C peptides in phosphate and TRIS buffers.

Optimizing Methods for smFRET

Develop a Method to Allow the Simultaneous Tracking of Two Fluorophores Using a Single EMCCD Digital Camera.

To successfully perform smFRET, we required a system that could track the intensity of two different fluorophores emitting in two different channels of wavelength simultaneously.

Data were recorded using the program Single, developed by the lab of Dr. Taekjip Ha. Single must be run in Administrative Mode however for it to function. We performed TIRF microscopy using the Nikkon microscope belonging to the lab of Dr. Seth Robia allowing us to use protocols already established at Loyola. However, for smFRET we required the ability to track multiple fluorophores simultaneously. Typical fluorophore emission measurements are done by taking a photo with a filter detecting a single fluorophore, changing filters, and then taking a photo with filters detecting the second fluorophore. As the delay inherent in both taking multiple images and swapping filters between images makes tracking FRET in real time impossible, we used an Optosplit II image splitter. This microscope attachment allows detection of the emission channels from both Alexa 488 and 594 simultaneously. Simultaneous fluorophore emission detection means that we can draw conclusions about dynamic protein conformational changes during data analysis.

However, we encountered multiple issues using the Optosplit II that needed optimization. First, to analyze smFRET data, we require a calibration done prior to each experiment using fluorescent beads. The fluorescent beads must be detected in both detection channels for creation of a successful calibration file which was a problem with our initial bead choices. Secondly, as the downstream software used to analyze smFRET data requires data in a very specific format, having the cube out of calibration resulted in unusable data.

Fluorescent Bead Choice.

We initially used Yellow-green FluoSphere Fluorescent Microspheres from Thermo Fisher which resulted in very bright signal in the green emission channel while being barely

detectable in the red channel. To troubleshoot this issue, we tried multiple approaches. First, we tried red FluoSpheres already owned by the lab which simply reversed the issue by causing extremely bright signal in the red channel and were nearly undetectable in the green channel. Second, we tried a FluoSphere mixture borrowed from the Robia lab containing a variety of bead colors throughout the spectrum. At first, this mixture appeared to work to create a correlation between the two channels, but, as the mix contained beads that may only appear in one channel and the percentage of beads that appeared in both channels was quite low, the downstream software was unable to detect enough bright peaks in the sample to correctly create a mapping file.

While using the bead mixture, however, I noticed that the beads that regularly appeared equally in both channels were visibly orange under the microscope eyepiece (Figure 14). Based on this observation, we ordered orange FluoSpheres from Thermo which emit at 560nm which can be detected in both channels. The orange beads finally did result in a beads mapping file with a satisfactory number of peaks in both channels[49].

We also had problems caused by clumping of beads under some conditions leading to situations where distinct peaks were not easily distinguishable by software (Figure 15D-E). I pursued two hypotheses for why the beads may be clumping. In the first hypothesis, clumping could be caused by sealing the microfluidic chamber, a process most effectively done using hot wax which could potentially partially melt the latex beads and cause them to stick together. In my second hypothesis, clumping could be caused by buffer choice if certain salt ions caused the beads to aggregate. I found that chamber sealing method had no effect on bead clumping. No

differences were observed when sealing using wax versus leaving off any sealant. However, changing the buffer from the recommended .25M $MgCl_2$ solution to PBS only completely stopped aggregation. $MgCl_2$ is generally recommended in creation of bead calibration slides because the ions should help the beads adhere to the glass slide surface and reduce the frequency of beads diffusing in and out of the plane of TIRF focus. In slides using plain PBS, we did see beads moving in and out of the plane of focus more often, but generally enough beads were present in the plane of focus to create a calibration file.

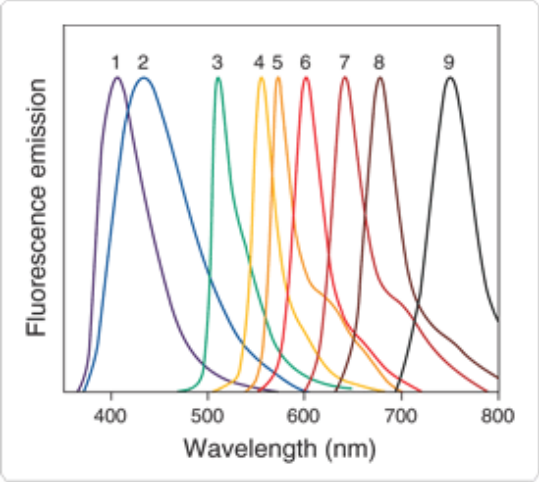

Figure 14. Fluorescent Bead Emission Spectra. Emission spectra of Thermo-Fisher FluoSphere beads. Of note for this document are 3: yellow-green (505/515), 4: orange (540/560), and 6: red (580/605). Spectra obtained from the Thermo-Fisher product website: https://tools.thermofisher.com/content/sfs/manuals/mp05000.pdf

Cube Calibration.

Splitting the emitted light into the two specific wavelengths we wanted to observe for smFRET required use of a device called an Optosplit II which must be kept in good calibration. The Optosplit II uses a setup of a dichroic mirror contained in a custom ordered cube from Cairn

Research combined with several other mirrors to split the collected light from the sample into the emission wavelengths from the donor and acceptor fluorophores (Figure 15A). For proper downstream analysis, the two channels should appear as two side-by-side rectangles on the output image that fill most of the image and split down the image center (Figure 15B-C). If the rectangles are tilted or off center, then downstream analysis will mostly turn out junk data or software errors (Figure 16).

Early on, we found that the Optosplit II does fairly quickly get out of correct alignment and that it is very easy to cause further alignment discrepancies while trying to fix the calibration. Once the matter of the fluorescent beads had been sorted out, it was necessary to properly calibrate the Optosplit mirrors. Initially, the Optosplit was far enough out of alignment that the rectangular output frames were concentrated only on one side of the image, a conformation the downstream software refused to even recognize. It also became apparent that the calibration instructions included with the Optosplitter were insufficient to properly perform calibration. After consultation with technicians at Cairn Research, the Optosplitter manufacturers, we learned that severe calibration issues could be addressed by removing the dichroic mirror cube, centering the output image, replacing the cube, and trying to shift the rectangles back into their correct positions. Because of how severely the Optosplitter was misaligned, we required multiple rounds of calibration before the Optosplitter was ready for use in smFRET.

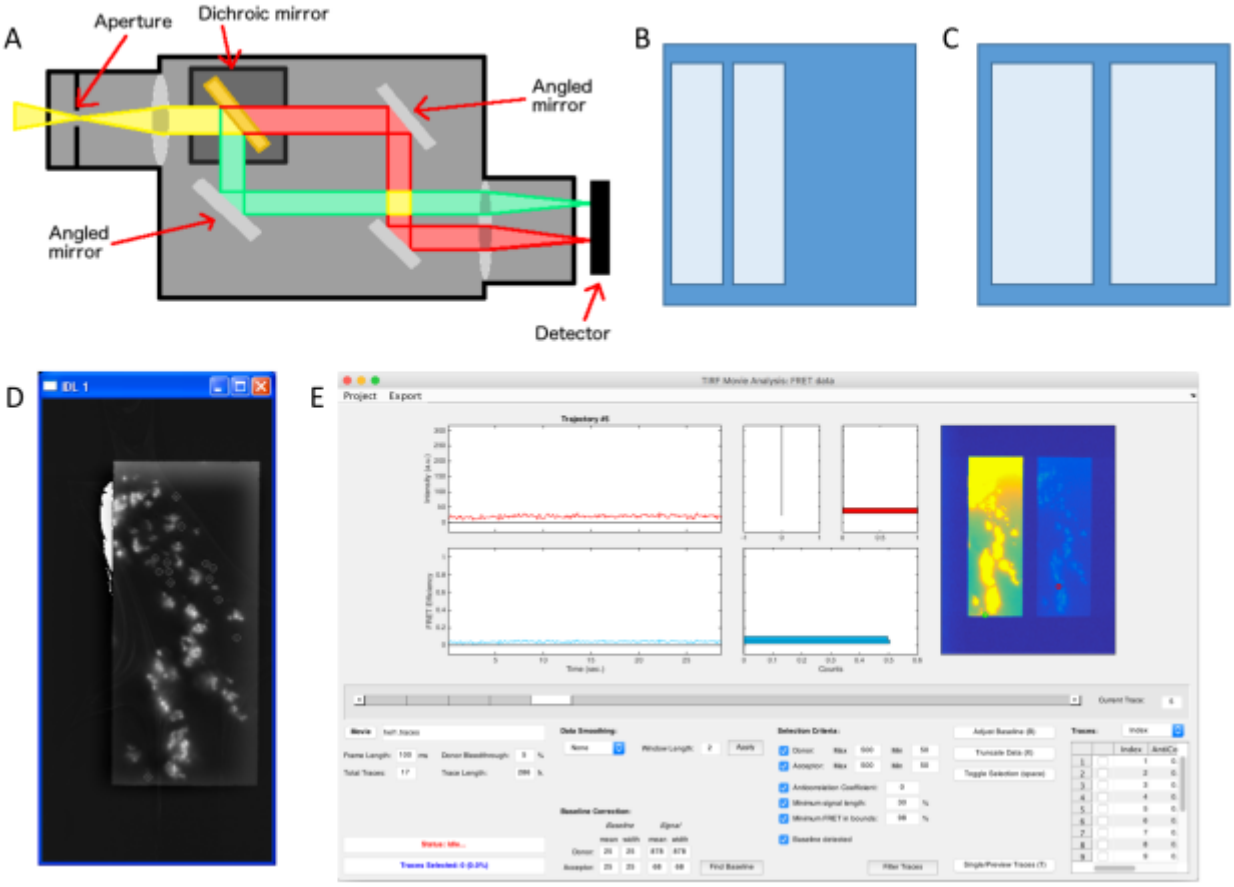

Figure 15. Optosplitter Calibration.
A: Diagram of the Optosplit II internal mirror setup and light paths.
B: Output of a seriously mis-calibrated Optosplit II with both emission windows on the left of the image.
C: Output of a properly calibrated Optosplit II with the emission windows split neatly down the middle and taking up most of their respective sides.
D: IDL attempt to align two emission windows. Note the clumping of the visible beads (not advisable) and the image shearing present on the left side. More difficult to see in this screenshot, one of the emission windows has been twisted like a spider web and is no longer remotely rectangular.
E: Matlab analysis resulting from the bead data collected in D. Note how the selection circles in the right window do not match up to the same location in the image.
Panel A drawn by Margret Bradley using the program GIMP.

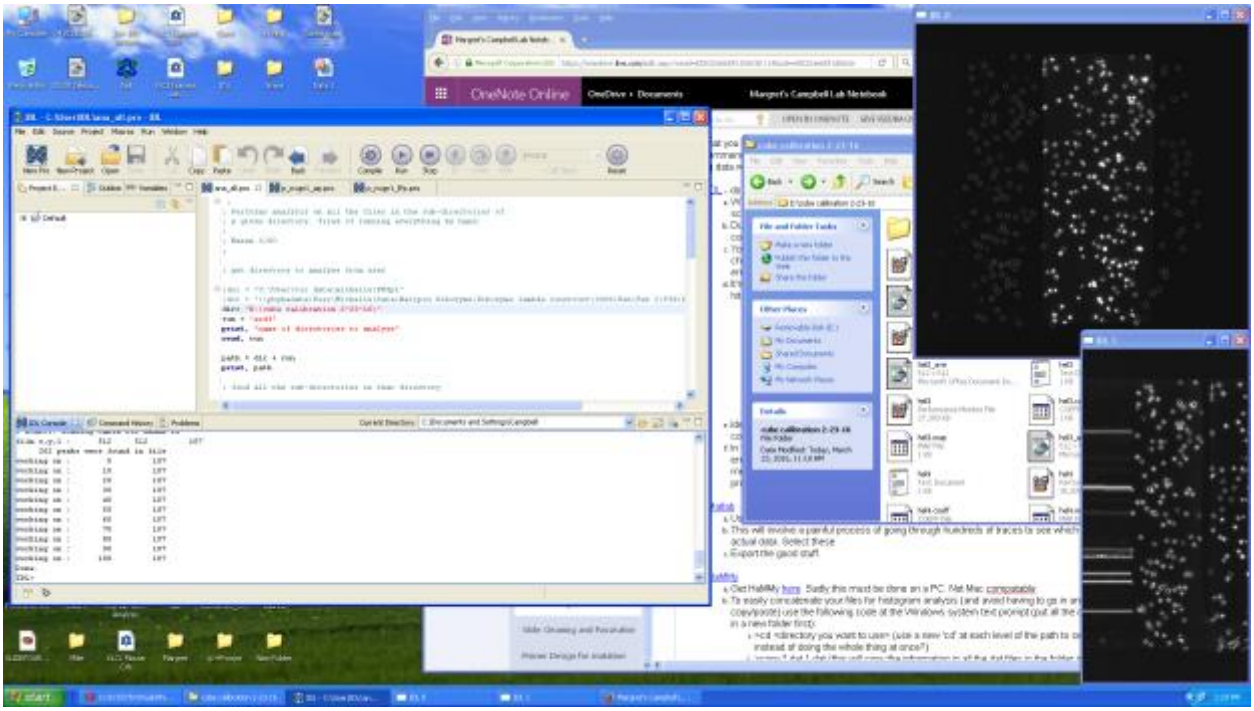

Figure 16. Optosplitter Calibration 2. IDL software attempting to align the two output windows and create a mapping file. Note here how the software is selecting spots in part of the image that contains no data at all and ignores many actually good matches. In the bottom right window, IDL attempted to place the two images on top of each other which resulted in severe image shearing and torqueing.

Establish a Workflow in IDL to Correctly Correlate the Two Wavelengths of Light Data Acquired from smFRET.

Once the data have been acquired, raw data must be converted into trace files for analysis. Conversion of raw data into trace files utilizes IDL software included with Single from the lab of Dr. Taekjip Ha. IDL, or Interactive Data Language, is a programming language used specifically for data analysis and must be licensed for use in the lab. The program set contains multiple subprograms. We used six of the subprograms for data analysis and found that properly using the programs required a level of comfort with code as IDL can be extremely

sensitive to input and easily produces program errors. IDL usage is discussed in detail in the smFRET Data Mapping section of the Methods.

The first IDL problem encountered by the lab was the file setup input requirements. While saving files, we typically saved experiments by having a main folder for the day containing multiple subfolders for the calibration and experimental slides examined during the day of experiments. Then, when trying to analyze the data in IDL, we could create a calibration file and get caught on the step where IDL attempts to analyze all the files in the folder. After reading the code, we discovered that the IDL program required a second layer of folders such that all data folders were contained in another folder which had all the data. IDL also produced errors if there were not enough bright peaks in the beads file or if the channel windows were not in the correct positions as discussed in the previous section.

Finally, IDL programs can be modified during data analysis to facilitate the analysis workflow such as entering new file paths into the program coding to direct the code at a new day's experiment. While this process largely acted as a method to ease analysis, failure to compile all the active programs could result in failure of the program. IDL was also extremely sensitive in terms of active window choice, largely during mapping file creation. If the incorrect window was selected while giving input commands, then the entire program would crash and need to be restarted.

In conclusion, correct choice of beads and spending the time to learn to calibrate the Optosplit II cube finally resulted in data that could be processed and analyzed.

Use Matlab to Render Acquired Data into Individual smFRET Traces and Graphs of Compiled smFRET Data.

Once the trace files had been generated, we could begin analysis of the data looking for meaningful patterns correlating to dynamic conformational protein changes observed. Trace files were loaded into Matlab programs developed by Raymond Pauszek in the lab of Dr. David Millar of the Scripps Research Institute.

Trace files were first filtered to select for several inclusion criteria. I chose traces that came from individual molecules as visible on the right side of the program, avoiding traces coming from more clumped areas. The traces were sorted by anti-correlation constant. The anti-correlation constant describes the behavior of the two light intensities on a scale of 0-1 with a score of 0 meaning the two fluorophores are behaving in an opposite manner wile a score of 1 means the fluorophores are acting in the same manner. We chose traces with anti-correlation constants closer to 0. We also chose traces with a distinct single-step photobleaching event. The photobleaching event helps support the hypothesis that you are looking at only one molecule as traces belonging to multiple molecules will display a curve downwards to the end of the trace due to multiple photobleaching events (Figure 17). Typically, 10-15 trace files were taken per sample and each trace file would contain several hundred molecule traces to sort through with only about 5% of the traces resulting in real data (Figure 18A). However, any improper setup in previous steps or poor conditions in the sample detection chamber could result in bad data that would only become apparent at this step, when we were finally able to look at the traces.

Once the good traces have been selected they can be exported and all traces from a single experiment combined. The traces must then be cropped to remove all data post photobleaching which should not be included in the final analysis[1]. Matlab can also draw histograms of FRET efficiencies from the data and fit curves to the histograms based on the number of peaks observed by the user (Figure 18B). HaMMY, another program from the lab of Dr. Taekjip Ha, can then be used to perform mass Hidden Markov modelling analysis to find the FRET efficiency levels in each trace[12]. These HaMMY files then are loaded into a final Matlab program which creates transition density plots (Figure 18C). Transition density plots allow examination of transfer between states. For example, if the sample is in a .2 FRET efficiency state and the other states available are .6 and .8, the sample has a percent chance to transfer to either the .6 or .8 states. The probability of moving from one state to another is shown on transition density plots.

In conclusion, Matlab analysis of smFRET data outputs meaningful graphs and figures that can be used to draw conclusions about the protein under study.

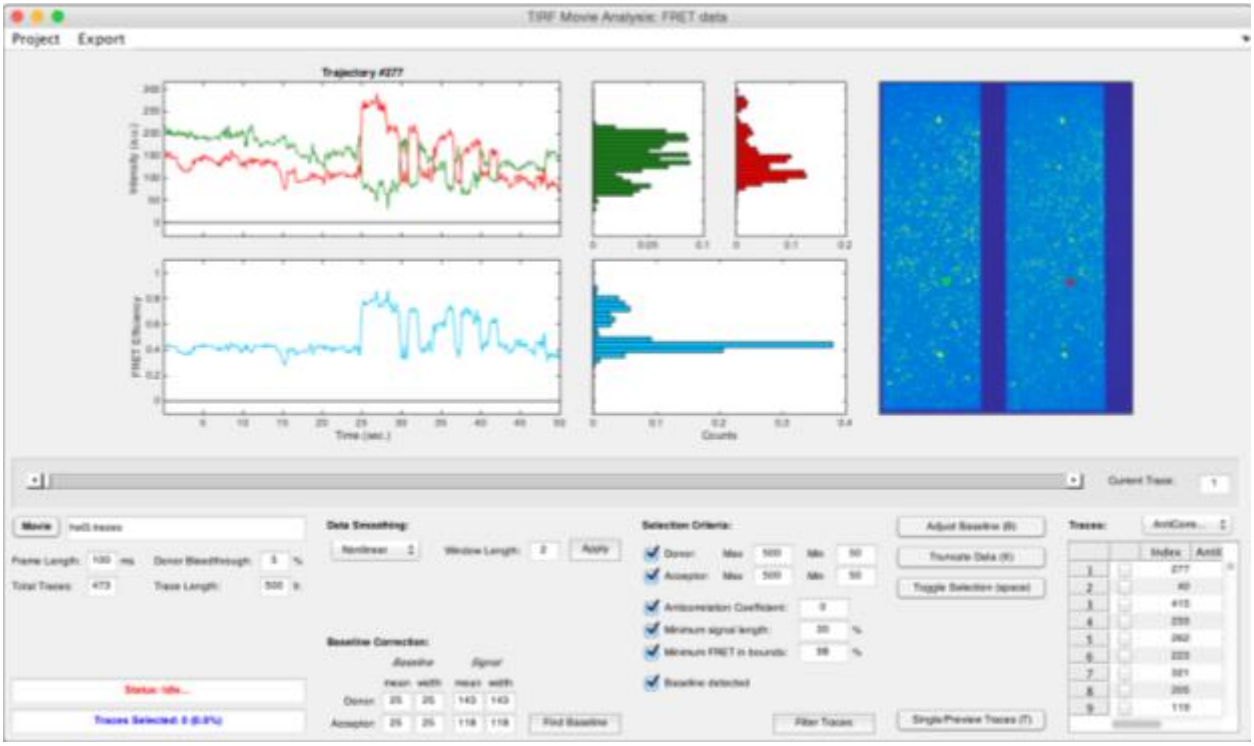

Figure 17. Rhesus CCL2-C Trace. One of the first successful trace files obtained independently by the Campbell

A

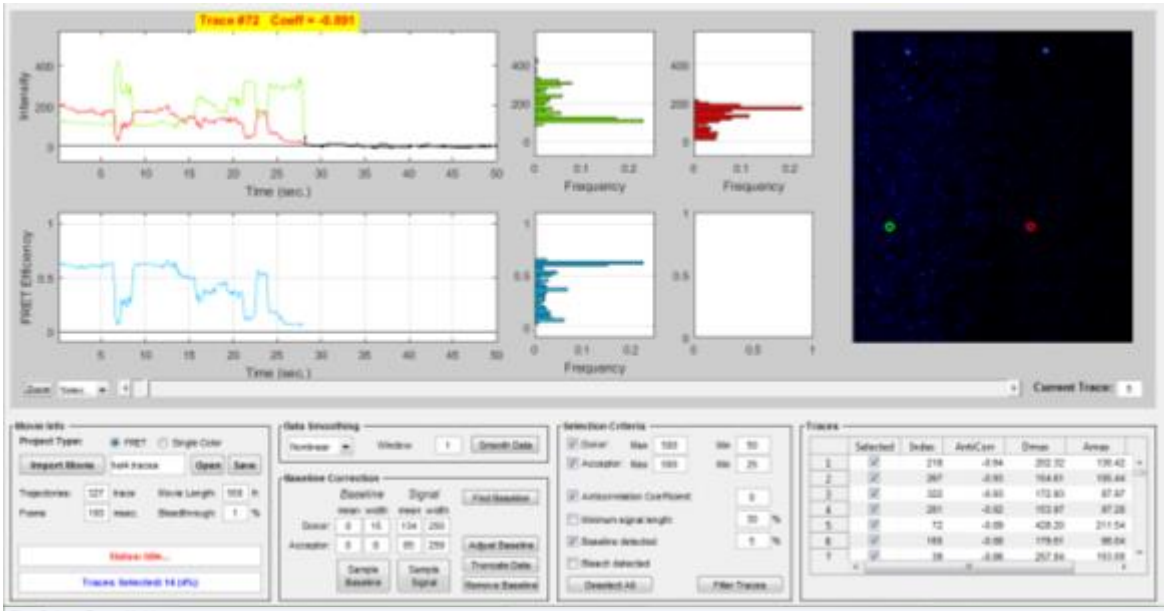

B

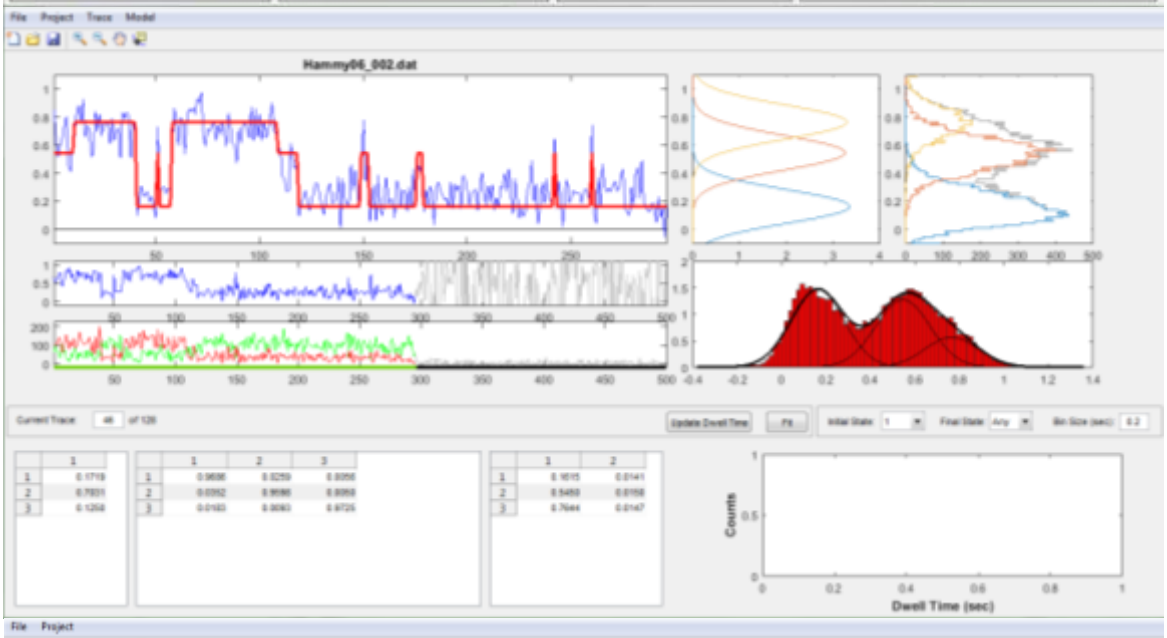

C

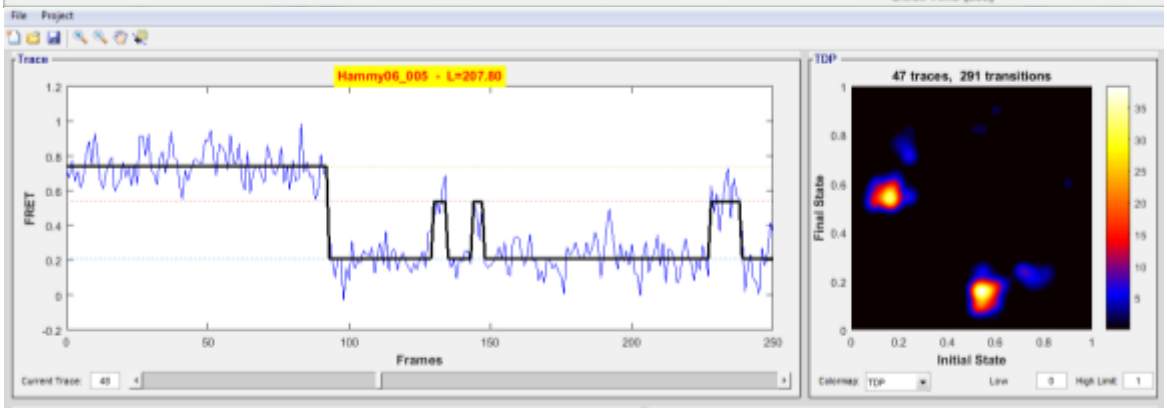

Figure 18. Matlab Analysis of smFRET Data.
A: Screenshot of the tirf_movieprocessing program where traces are first selected for quality. Notice the strong anti-correlation in the trace image shown with a distinct photobleach event. Data after the photobleaching event has been cropped which is shown where the FRET efficiency graph ends and the Intensity graph lines turn from green and red to black.
B: Screenshot of the vfit program where traces are compiled. The top left window shows preliminary Hidden Markov Modelling analysis which will be finalized in HaMMY. This program also show a histogram of the FRET efficiencies of the compiled data with curves fit to the observed peaks.
C: Screenshot of the viewhammy2 program which compiles the traces which have been analyzed in HaMMY into a transition density plot.

CHAPTER IV: DISCUSSION

Single-molecule FRET is a relatively new method used in only a handful of labs to study dynamic interactions on the scale of single proteins[1]. Using FRET between small fluorophores conjugated to specific sites on proteins, smFRET can reveal conformational changes occurring in real time at high specificity[47]. We in the Campbell Lab sought to adapt smFRET methods for use at Loyola to study a variety of proteins. To analyze proteins via smFRET, we first needed to create, purify, and label proteins suitable for smFRET. We then needed to optimize several new protocols for smFRET that had never been used before in the Campbell Lab.

We first tackled creating a peptide for smFRET study using the CC and L2 domains of the protein TRIM5α. We tagged a cysteine onto the peptide C-terminus for site-specific fluorophore conjugation. We found that purification of the CCL2-C protein required only purification of the soluble protein from the lysed bacterial cell supernatant via the 6-His tag. We then optimized and simplified the method for conjugation of maleimide-linked small fluorophores to the purified CCL2-C proteins by combining the fluorophores when conjugating them to the proteins and removing several days of dialysis. Our improved protocol also limits risk of misfolding the proteins during re-naturation. We analyzed our purified proteins using a combination of coomassie, typhoon imaging, and circular dichroism. These analyses showed that the protein largely existed as monomers or denaturable dimers after purification, that fluorescent labelling was successful, and that the purified proteins generally had the expected secondary structure.

We then addressed adapting smFRET specific methods for our lab. While TIRF was already established using the microscope from the lab of Dr. Seth Robia, several methods for smFRET were not. One of the chief problems we needed to handle was creating data acceptable for use by downstream software. The Optosplit II device, which allows us to observe two light emission channels simultaneously, became an obstacle to overcome due to the technical difficulty of getting the Optosplit II unit into calibration. We also needed to choose a fluorescent bead type for mapping the images generated by the two channels onto each other which was resolved by selecting orange beads. The orange beads have an emission peak between the two channels detected by the Optosplit II dichroic mirror we used. Since fluorescent beads are very bright, their emission appeared at relatively even levels in both the red and green light detection channels.

Analysis of smFRET data requires use of software acquired from labs where smFRET is already established, but, to get the programs to work for our lab and our project, the data needed to be set up to input into the programs correctly and the programs needed to be modified to produce the desired output. IDL, the program used to process the raw data files, required very specific input file formats which were not always made clear in the supporting material. Therefore, some software language knowledge from the user was required to read the IDL code and determine where errors were occurring and correct them. Finally, we established a workflow in Matlab to filter the large quantities of data generated in an experiment and compile the data into meaningful graphs and charts so that conclusions about the protein could be drawn.

Conclusion

In conclusion, we developed a protocol to use single-molecule FRET (smFRET) in the Campbell Lab at Loyola University Chicago. smFRET is a complex method that allows scientists to examine conformational changes occurring in single biological macromolecules in real time. While we used two domains or the protein TRIM5α, this protocol can now be used at Loyola University Chicago to study any protein, DNA, or RNA complex that can be adhered to a glass slide and conjugated to fluorescent proteins. Thus the results of this thesis will help scientific research in a continuing manner in the Campbell Lab.

REFERENCE LIST

1. Roy, R., Hohng, S. & Ha, T. A Practical Guide to Single Molecule FRET. doi:10.1038/nmeth.1208

2. Munro, J. B. *et al.* Conformational dynamics of single HIV-1 envelope trimers on the surface of native virions. *Science (80-.).* **346,** 759–763 (2014).

3. Berezhna, S. Y., Gill, J. P., Lamichhane, R. & Millar, D. P. Single-Molecule Förster Resonance Energy Transfer Reveals an Innate Fidelity Checkpoint in DNA Polymerase I. *J. Am. Chem. Soc.* **134,** 11261–11268 (2012).

4. Bunt, G. & Wouters, F. S. FRET from single to multiplexed signaling events. *Biophys. Rev.* **9,** 119–129 (2017).

5. Kim, Y. *et al.* Efficient site-specific labeling of proteins via cysteines. *Bioconjug. Chem.* **19,** 786–91 (2008).

6. Joo, C. & Ha, T. Preparing Sample Chambers for Single-Molecule FRET. *Cold Spring Harb. Protoc.* **2012,** pdb.prot071530-prot071530 (2012).

7. Juvaste, H., Iiskola, E. I. & Pakkanen, T. T. Aminosilane as a coupling agent for cyclopentadienyl ligands on silica. *J. Organomet. Chem.* **587,** 38–45 (1999).

8. Joo, C. & Ha, T. Objective-Type Total Internal Reflection Microscopy (Excitation) for Single-Molecule FRET. *Cold Spring Harb. Protoc.* **2012,** pdb.prot072025-prot072025 (2012).

9. Joo, C. & Ha, T. Objective-Type Total Internal Reflection Microscopy (Emission) for Single-Molecule FRET. *Cold Spring Harb. Protoc.* **2012,** pdb.prot072033-prot072033 (2012).

10. Joo, C. & Ha, T. Prism-Type Total Internal Reflection Microscopy for Single-Molecule FRET. *Cold Spring Harb. Protoc.* **2012,** pdb.prot072041-prot072041 (2012).

11. Rusinova, E., Tretyachenko-Ladokhina, V., Vele, O. E., Senear, D. F. & Alexander Ross, J. B. Alexa and Oregon Green dyes as fluorescence anisotropy probes for measuring protein–protein and protein–nucleic acid interactions. *Anal. Biochem.* **308,** 18–25 (2002).

12. Okamoto, K. in *Methods in molecular biology (Clifton, N.J.)* **1552,** 103–113 (2017).

13. Gallo, R. C. & Montagnier, L. The Discovery of HIV as the Cause of AIDS. *N. Engl. J. Med.* **349,** 2283–2285 (2003).

14. Becerra, J. C., Bildstein, L. S. & Gach, J. S. Recent Insights into the HIV/AIDS Pandemic. *Microb. Cell* **3,** 450–474 (2016).

15. WHO | HIV/AIDS. *WHO* (2016).

16. Lackner, A. A., Lederman, M. M. & Rodriguez, B. HIV pathogenesis: the host. *Cold Spring Harb. Perspect. Med.* **2,** a007005 (2012).

17. Goujard, C. *et al.* Continuous versus intermittent treatment strategies during primary HIV-1 infection: the randomized ANRS INTERPRIM Trial. *AIDS* **26,** 1895–905 (2012).

18. Siliciano, R. F. & Greene, W. C. HIV Latency. *Cold Spring Harb. Perspect. Med.* **1,** a007096–a007096 (2011).

19. Ozato, K., Shin, D.-M., Chang, T.-H. & Morse, H. C. TRIM family proteins and their emerging roles in innate immunity. *Nat. Rev. Immunol.* **8,** 849–860 (2008).

20. Reymond, A. *et al.* The tripartite motif family identifies cell compartments. *EMBO J.* **20,** 2140–51 (2001).

21. Bieniasz, P. D. Intrinsic immunity: a front-line defense against viral attack. *Nat. Immunol.* **5,** 1109–15 (2004).

22. Stremlau, M. *et al.* The cytoplasmic body component TRIM5alpha restricts HIV-1 infection in Old World monkeys. *Nature* **427,** 848–53 (2004).

23. Sanchez, J. G. *et al.* The tripartite motif coiled-coil is an elongated antiparallel hairpin dimer. *Proc. Natl. Acad. Sci. U. S. A.* **111,** 2494–9 (2014).

24. Diaz-Griffero, F. *et al.* A B-box 2 surface patch important for TRIM5alpha self-association, capsid binding avidity, and retrovirus restriction. *J. Virol.* **83,** 10737–51 (2009).

25. Ganser-Pornillos, B. K. *et al.* Hexagonal assembly of a restricting TRIM5 protein. *Proc. Natl. Acad. Sci.* **108,** 534–539 (2011).

26. Wagner, J. M. *et al.* Mechanism of B-box 2 domain-mediated higher-order assembly of the retroviral restriction factor TRIM5α. *Elife* **5,** (2016).

27. Keown, J. R., Goldstone, D. C. & Goldstone, D. C. Crystal structure of the Trim5Î± Bbox2 domain from rhesus macaques describes a plastic oligomerisation interface. *J. Struct. Biol.* (2016). doi:10.1016/j.jsb.2016.07.004

28. Biris, N. *et al.* Structure of the rhesus monkey TRIM5 PRYSPRY domain, the HIV capsid recognition module. *Proc. Natl. Acad. Sci.* **109,** 13278–13283 (2012).

29. Stremlau, M., Perron, M., Welikala, S. & Sodroski, J. Species-specific variation in the B30.2(SPRY) domain of TRIM5alpha determines the potency of human immunodeficiency virus restriction. *J. Virol.* **79,** 3139–45 (2005).

30. Biris, N., Tomashevski, A., Bhattacharya, A., Diaz-Griffero, F. & Ivanov, D. N. Rhesus monkey TRIM5α SPRY domain recognizes multiple epitopes that span several capsid monomers on the surface of the HIV-1 mature viral core. *J. Mol. Biol.* **425,** 5032–44 (2013).

31. Goldstone, D. C. *et al.* Structural studies of postentry restriction factors reveal antiparallel dimers that enable avid binding to the HIV-1 capsid lattice. *Proc. Natl. Acad. Sci. U. S. A.* **111,** 9609–14 (2014).

32. Tareen, S. U. & Emerman, M. Human Trim5α has additional activities that are uncoupled from retroviral capsid recognition. *Virology* **409,** 113–20 (2011).

33. Yap, M. W., Nisole, S. & Stoye, J. P. A single amino acid change in the SPRY domain of human Trim5alpha leads to HIV-1 restriction. *Curr. Biol.* **15,** 73–8 (2005).

34. Richardson, M. W., Guo, L., Xin, F., Yang, X. & Riley, J. L. Stabilized human TRIM5α protects human T cells from HIV-1 infection. *Mol. Ther.* **22,** 1084–95 (2014).

35. Bieniasz, P. D. Restriction factors: a defense against retroviral infection. *Trends Microbiol.* **11,** 286–91 (2003).

36. Stremlau, M. *et al.* Specific recognition and accelerated uncoating of retroviral capsids by the TRIM5? restriction factor. *Proc. Natl. Acad. Sci.* **103,** 5514–5519 (2006).

37. Diaz-Griffero, F. *et al.* Rapid turnover and polyubiquitylation of the retroviral restriction factor TRIM5. *Virology* **349,** 300–15 (2006).

38. Rold, C. J. & Aiken, C. Proteasomal Degradation of TRIM5α during Retrovirus Restriction. *PLoS Pathog.* **4,** e1000074 (2008).

39. Diaz-Griffero, F. *et al.* Modulation of retroviral restriction and proteasome inhibitor-resistant turnover by changes in the TRIM5alpha B-box 2 domain. *J. Virol.* **81,** 10362–78 (2007).

40. Campbell, E. M., Perez, O., Anderson, J. L. & Hope, T. J. Visualization of a proteasome-independent intermediate during restriction of HIV-1 by rhesus TRIM5alpha. *J. Cell Biol.* **180,** 549–61 (2008).

41. Wu, X., Anderson, J. L., Campbell, E. M., Joseph, A. M. & Hope, T. J. Proteasome inhibitors uncouple rhesus TRIM5alpha restriction of HIV-1 reverse transcription and infection. *Proc. Natl. Acad. Sci. U. S. A.* **103,** 7465–70 (2006).

42. Imam, S. *et al.* TRIM5α Degradation via Autophagy Is Not Required for Retroviral Restriction. *J. Virol.* **90,** 3400–10 (2016).

43. Campbell, E. M. *et al.* TRIM5α-Mediated Ubiquitin Chain Conjugation Is Required for Inhibition of HIV-1 Reverse Transcription and Capsid Destabilization. *J. Virol.* **90,** 1849–57 (2015).

44. Imam, S. *et al.* TRIM5α Degradation via Autophagy Is Not Required for Retroviral Restriction. *J. Virol.* **90,** 3400–3410 (2016).

45. Lamichhane, R. *et al.* Dynamic conformational changes in the rhesus TRIM5α dimer dictate the potency of HIV-1 restriction. *Virology* **500,** 161–168 (2017).

46. Sastri, J. *et al.* Identification of residues within the L2 region of rhesus TRIM5alpha that are required for retroviral restriction and cytoplasmic body localization. *Virology* **405,** 259–66 (2010).

47. Munro, J. B. *et al.* Conformational dynamics of single HIV-1 envelope trimers on the surface of native virions. *Science* **346,** 759–63 (2014).

48. Johnson, W. C. Analyzing protein circular dichroism spectra for accurate secondary structures. *Proteins Struct. Funct. Genet.* **35,** 307–312 (1999).

49. MP 05000 FluoSpheres ® Fluorescent Microspheres Quick Facts FluoSpheres ® Fluorescent Microspheres.

VITA

The author, Margret Bradley, was born in Manchester, CT on November 10, 1990 to Michael and Katherine Bradley. She attended St. Olaf College in Northfield, MN where she earned a Bachelor's of Arts, in Biological Sciences in June 2013. After graduation, Margret worked a year at Epic testing hospital software before matriculating into the Loyola University Chicago Stritch School Microbiology and Immunology Graduate Program. After completing one year of graduate school, she began her graduate education in the Microbiology and Immunology Program. In the spring of 2015, Margret joined the lab of Dr. Ed Campbell in the department of Microbiology and Immunology. Margret's thesis work focused on developing single-molecule FRET methods to study dynamic conformational changes in proteins on a molecular level.

After graduation, Margret plans to seek employment in industry research or the forensic sciences.

Figure 19. Performing Single-Molecule FRET.
Hand drawn by Margret Bradley